



Similarities in the rupture process and cascading asperities between neighboring fault patches and seismic implications: The 2002–2009 Sumbawa (Indonesia) earthquakes with moment magnitudes of 6.2–6.6

Dimas Sianipar^{a,c,e}, Bor-Shouh Huang^{b,c,*}, Kuo-Fong Ma^{b,d}, Ming-Che Hsieh^d, Po-Fei Chen^c, D. Daryono^e

^a Taiwan International Graduate Program (TIGP) Earth System Sciences, Academia Sinica and National Central University, Taipei, Taiwan

^b Institute of Earth Sciences, Academia Sinica, Taipei, Taiwan

^c Department of Earth Sciences, National Central University, Taoyuan, Taiwan

^d Earthquake-Disaster & Risk Evaluation and Management Center (E-DREaM), National Central University, Taoyuan, Taiwan

^e Agency for Meteorology, Climatology, and Geophysics of the Republic of Indonesia (BMKG), Jakarta, Indonesia

ARTICLE INFO

Keywords:

Asperities
Finite-fault
Flores Thrust
Rupture
Source-time-functions

ABSTRACT

The Flores Thrust is a southward-dipping, low-to-moderate angle submarine active fault in the eastern Sunda-Banda back-arc (Indonesia). Significant shallow-depth destructive earthquakes have been reported along this fault zone. From 2002 to 2009, one of its fault segments, called the Sumbawa segment, experienced five earthquakes with moment magnitude (M_W) values of 6.2–6.6. In this study, we performed finite-fault rupture inversions for these earthquakes, constrained with teleseismic body and surface waveforms, to investigate the characteristics of earthquake ruptures along this fault zone. We obtained the source-time-functions and finite-fault rupture models for these five earthquakes. Results indicated that ruptures often propagated along-strike or down-dip. The ruptures were initiated from the middle crust (depth of approximately 12–17 km) and exhibited a comparable initiation behavior to their entire rupture. The rupture speeds and stress drops were approximately 2.0–2.5 km/s and 1.0–2.0 MPa, respectively. Five cascading asperities ruptured neighboring fault patches and did not overlap each other. The characteristics of earthquake source parameters and rupture processes obtained in this study are robust and helpful for future regional seismic hazard assessment and earthquake early warning studies. These cascading asperities might be related to the fault immaturity of the western Flores Thrust. Alternatively, these earthquakes may act as asperities located at the down-dip patches of the Sumbawa segment, and its shallower section still has a potential of ruptures with $M_W > 7.0$.

1. Introduction

The Flores Thrust and Wetar Thrust are continuous active back-arc thrust faults located beyond the plate boundary in the eastern Sunda-Banda arc (Indonesia) (Koulali et al., 2016; Silver et al., 1983; McCaffrey and Nábělek, 1984). The Flores Thrust, which extends from the north of Flores Island to the west to Sumbawa, Lombok, and Bali Islands, is an active, long, southward-dipping fault (Fig. 1). The eastern part of this fault ruptured during the 1992 Flores earthquake with a moment magnitude (M_W) of 7.7 (Beckers and Lay, 1995; Pranantyo and Cummins, 2019). This 1992 earthquake caused considerable destruction and generated a damaging tsunami. Further to the east, the Wetar Thrust was

also ruptured by a large earthquake ($M_W = 7.5$) that occurred in 2004 (Hayes, 2017; <https://earthquake.usgs.gov/earthquakes/eventpage/us000d85g/>). A zone between the north of Bali and Lombok Island was previously considered as the westernmost termination of the Flores Thrust zone (McCaffrey and Nábělek, 1987; Silver et al., 1983). However, the geodetic modeling findings of a previous study suggested that the Flores Thrust can extend further west, probably linking with the Kendeng Fault Zone in Java Island (Koulali et al., 2016). Furthermore, whether the western part of the Flores Thrust can experience a large earthquake ($M_W > 7$) similar to its eastern part remains unclear.

The Flores Thrust often experiences shallow, destructive, and moderate-to-large magnitude earthquakes. From 2002 to 2009, a

* Corresponding author at: Institute of Earth Sciences, Academia Sinica, Taipei, Taiwan.

E-mail address: hwbs@earth.sinica.edu.tw (B.-S. Huang).

<https://doi.org/10.1016/j.jseas.2022.105167>

Received 9 July 2021; Received in revised form 17 February 2022; Accepted 25 February 2022

Available online 28 February 2022

1367-9120/© 2022 Elsevier Ltd. All rights reserved.

sequence of damaging earthquakes (five earthquakes with $M_W > 6$) struck north of Sumbawa Island (Fig. 1). Table 1 lists the source origin times and epicenters of those five events. The reported epicenters and focal mechanisms of these earthquakes fit well with their occurrence along the Flores Thrust; however, the detailed source processes of these earthquakes have not been well investigated and their further implications have not been discussed. In addition to limited observations, seismological studies on the Sumbawa part of the Flores Thrust are lacking. Recently, Fuchs et al. (2014) found a possible triggered nonvolcanic tremor in the Flores Thrust, Sumbawa segment. The most recent studies conducted in this region have focused on the destructive earthquakes that occurred in the north of Lombok Island in 2018 (Lythgoe et al., 2021; Wang et al., 2020). Given the 2002–2009 Sumbawa earthquake records, some critical questions need to be addressed to evaluate seismic and tsunami hazards in this region. For example, the rupture characteristics and seismogenic behavior of shallow, destructive earthquakes in Sumbawa were not well known.

In this study, we performed a detailed seismological analysis of five Sumbawa earthquakes (with M_W ranging from 6.2 to 6.6) that occurred between 2002 and 2009. We inverted finite-fault rupture models and visualized their moment rate functions. The moment rate function that is often referred to as the source-time-function (STF) of an earthquake was considered in this study. Furthermore, we evaluated source parameters, namely the rupture initiation, size, speed, and stress drop, from obtained

finite-fault rupture models. In addition, we discussed the regional seismotectonic implications of our findings. The findings of this study can be applied to future seismic and tsunami hazard assessments, particularly for earthquakes in Sumbawa Island (Irsyam et al., 2020; Yuliastuti et al., 2021).

2. Data

A catalog of teleseismically well-constrained seismicity from the ISC-EHB database was referred to for understanding the regional seismic activity of the study region (Engdahl et al., 2020). This catalog provides accurate data regarding relocated events from 1964 to 2017 with their spatial resolutions (Fig. 1a and 1b). Seismicity on the Flores Thrust was found to be isolated from seismic activities along the Java Trench and Indo-Australian subducted slab (Fig. 1b). However, major observations of ISC-EHB catalog events were from teleseismic distances; small events could not be identified, and the depth uncertainty of hypocenters was usually approximately 10 km (Engdahl et al., 2020). Local/regional earthquakes compiled by the Indonesian Agency for Meteorology, Climatology, and Geophysics (BMKG) have been available since 2009 and were also referred to in this study (Fig. 1c). As shown in Fig. 1c, double-couple focal mechanisms of the five analyzed events retrieved from the Global Centroid Moment Tensor (CMT) database were included (Ekström et al., 2012). These data were used for constructing the fault

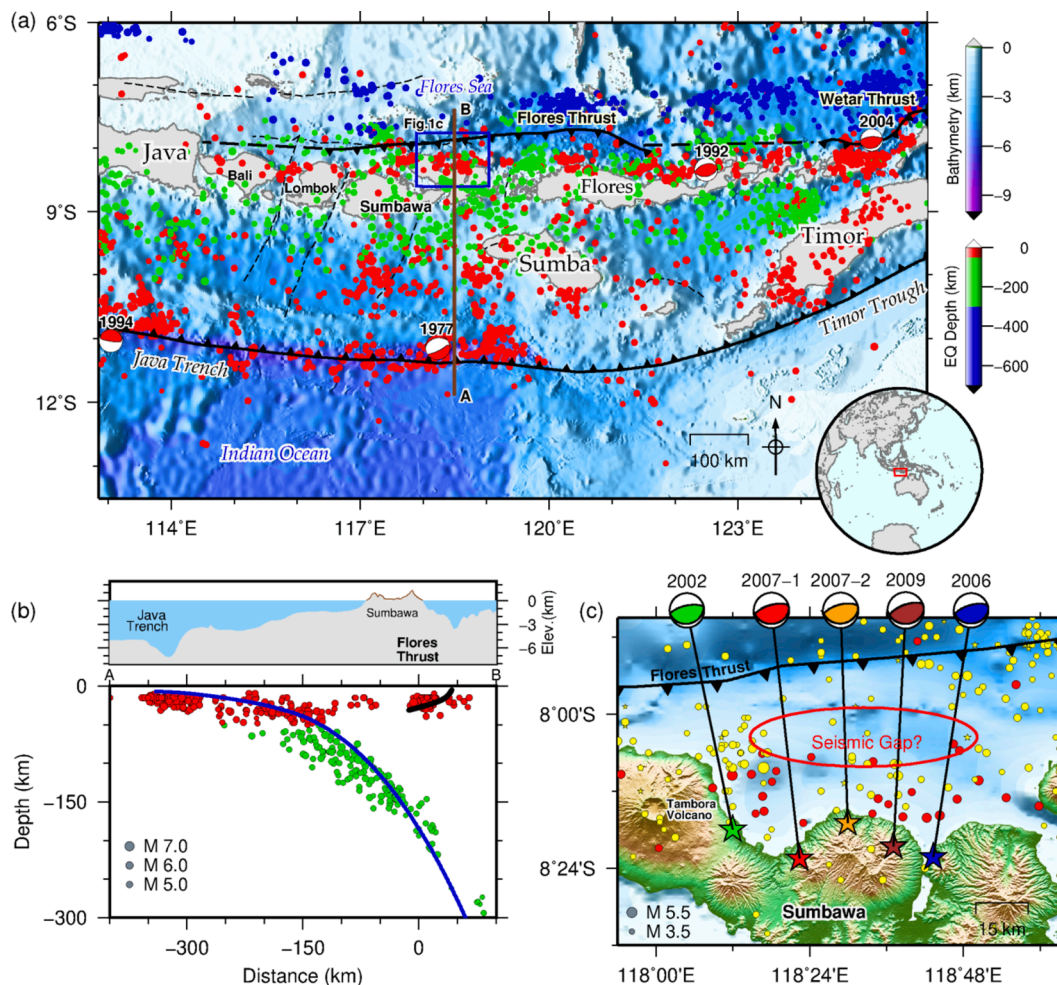


Fig. 1. (a) Tectonic setting of the 2002–2009 Sumbawa earthquakes. The relocated seismicity from the ISC-EHB catalog is shown (Engdahl et al., 2020); red, green, and blue represent depths of < 50 km, $50\text{--}300$ km, and >300 km, respectively. Fig. 1c is an enlargement of the blue box. Beachballs depict earthquakes with $M_W > 7.5$ according to global CMT. (b) South–north cross-section showing the location of the Flores Thrust relative to the plate boundary (subduction zone). (c) Enlargement of area of the 2002–2009 Sumbawa earthquakes. Beachballs show double-couple focal mechanisms of large earthquakes ($M_W \geq 6.2$) during 2002–2009 (global CMT catalog) (Ekström et al., 2012). The yellow circles show recent regional shallow seismicity ($M_L > 3.5$, depth < 50 km) from the BMKG catalog during 2009–2020.

Table 1
Source parameters of the 2002–2009 Sumbawa earthquakes.

Parameter	2002	2006	2007–1	2007–2	2009
Origin Time (UTC)	2002–10-06 15:46:35.1	2006–12-01 14:01:45.4	2007–11-25 16:02:16.0	2007–11-25 19:53:05.7	2009–11-08 19:41:43.7
Epicenter (ISC-EHB)	8.30°S, 118.20°E	8.37°S, 118.72°E	8.38°S, 118.37°E	8.28°S, 118.50°E	8.34°S, 118.62°E
Seismic moment in Nm from GCMT, (M_w)	2.67×10^{18} , (6.2)	4.00×10^{18} , (6.3)	6.11×10^{18} , (6.5)	6.15×10^{18} , (6.5)	1.08×10^{19} , (6.6)
Seismic moment in Nm from this study, (M_w)	2.45×10^{18} , (6.2)	3.60×10^{18} , (6.3)	5.51×10^{18} , (6.4)	5.72×10^{18} , (6.4)	9.74×10^{18} , (6.6)
Initiation depth (km)	14	17	15	12	15
Peak slip (cm)	56	55	105	73	142
Average slip (cm)*	27 (24)	29 (24)	47 (42)	32 (29)	67 (62)
Effective length (km)*	16.6 (20.0)	20.8 (27.5)	17.8 (20.0)	21.7 (22.5)	17.9 (20.0)
Effective width (km)*	13.9 (17.5)	15.0 (17.5)	16.4 (20.0)	23.5 (25.0)	20.5 (25.0)
Rupture duration (s)	7	10	8	11	12
Static stress drop (MPa)	1.0	1.1	1.6	0.7	2.0

* Numbers in brackets show the result obtained by trimming subfaults with <17% of the peak slip (Ye et al., 2016).

geometries of the earthquake rupture process for the analyzed events.

High-quality seismic waveform data were obtained from the Global Seismographic Network for stations within a distance of 30°–90° (Fig. 2). Furthermore, additional data from the French Global Network of Seismological Broadband Stations and Germany GEOFON Program were collected. We converted all data into displacement seismograms and removed their instrument responses. For body waves (P and SH waves), a band-pass filter was applied to seismograms with frequency bands of 0.01 and 1 Hz. To obtain long-period surface waves, we filtered the data with a frequency range of 0.004–0.006 Hz (Hao et al., 2013). Fig. 2 shows an example of the body and surface waveforms of the five analyzed events in four selected stations. The filtered displacement seismograms of the five events from each selected station were similar, indicating the similarity of their source processes. All selected stations presented satisfactory azimuthal coverages (Fig. 2), and their seismic waveforms showed a favorable signal-to-noise ratio (seismograms can be found in the supplementary file).

During the period of the 2002–2009 Sumbawa earthquake sequence, no local or regional broadband seismic network or strong-motion instruments records are available to examine the seismic source rupture in detail. Only an operated regional broadband station (station II KAPI located at Sulawesi Island) with an epicentral distance of approximately 380 km has recorded this earthquake sequence well. In this study, we performed an empirical Green's function (EGF) analysis with data collected from station KAPI to confirm the results of this teleseismic inversion of this study.

3. Methods

In this study, we utilized finite-fault rupture inversion that involves wavelet domain transformation and the nonlinear simulated annealing method (Ji et al., 2002, 2003; Liu and Yao, 2018; Shao et al., 2011). Inversions were constrained using displacement seismograms for teleseismic body waves (P and SH waves) and surface waves (Rayleigh and Love waves) (Shao et al. 2011). This method involved simultaneously inverting the slip amplitude, rake angle, rupture initiation time, and the shape of an asymmetric cosine function for subfaults (Ji et al. 2003). The slip rate at each subfault was defined by the value of the starting time (t_s) and ending time (t_e) of this asymmetric cosine function (Ji et al. 2003). The inverted risetime (i.e., the local slip duration) was calculated by summing these times ($t_s + t_e$). The value of inverted risetime for each subfault was limited between 0.6 and 4.2 s.

We designed single rectangular fault planes on the basis of geometry defined by the global CMT double-couple solution (Fig. 1c). From two nodal planes, we selected the one that was striking to the east, southward dipping with a low-to-moderate angle, that matched with the geometry of the Flores Thrust (Lythgoe et al., 2021; McCaffrey and Nábělek, 1984; Silver et al. 1983; Yang et al. 2020). The initial size of the fault plane was first estimated based on the scaling relationship reported by Wells and Coppersmith (1994), and we doubled the size to account

for uncertainties in the rupture propagation direction (Hayes, 2017). Subsequently, we divided the fault plane into 2.5×2.5 -km subfault grids. We performed a series of initial inversions and adjusted the fault plane size. Then, we set the rupture to start from the epicenter defined on the basis of ISC-EHB relocated catalog events. Because hypocenter depths (i.e., rupture initiation depths) for the events varied substantially between earthquake catalogs, we adopted a grid-search approach with an interval of 1 km to determine the best rupture initiation depth (Lin et al. 2019; Yamanaka and Kikuchi, 2003). The vertical grid-search approach was performed for the same fault plane size, and we allowed the changes of individual parameters to obtain the best waveform fits between observed waveforms and synthetic seismograms including depth phases. For each subfault, we searched the rake angle (slip vectors) within the range of 0° to 180° to allow for all possible thrust movements. By contrast, Lin et al. (2019) used rake angles varying within $\pm 30^\circ$ of the global CMT rake. We varied the rupture speed from 1.25 to 3.75 km/s with a reference of 2.5 km/s based on a temporal constraint (Shao et al. 2011).

Body wave synthetic seismograms were computed using a teleseismic Green's function method (Helmberger, 1983; Langston and Helmberger, 1975). The synthetics for long-period surface waves were computed using the normal mode superposition algorithm (Gilbert and Dziewonski, 1975; Shao et al. 2011). Computations were performed using a seismic velocity model from CRUST 2.0 (Bassin et al. 2000; <https://igppweb.ucsd.edu/~gabi/crust2.html>), interpolated with the PREM model (Dziewonski and Anderson, 1981). We used the common teleseismic average attenuation factors $t^*_\alpha = 1.0$ s (for P waves) and $t^*_\beta = 4.0$ s (for SH waves). Finally, we inverted the finite-fault rupture models of the five Sumbawa earthquakes that included the spatial and temporal information of a two-dimensional fault rupture evolution. The moment rate function, rupture snapshots, and final fault plane slip distribution were determined from the finite-fault rupture model.

In addition to original procedures reported by Ji et al. (2002) and Shao et al. (2011), we performed statistical resampling tests to explore the stability and precision of results (Hartzell et al. 2007; Hayes, 2011; Shao and Ji, 2012; Tichelaar and Ruff, 1989) by using a so-called “leave one out” jackknife procedure. We systematically deleted one observation from our original dataset (i.e., sampling without replacement) and repeated the inversions (approximately 150 times). This resampling was repeated until all seismic traces were missing from one inversion dataset. Then, we evaluated the average and standard deviation (σ) of the inverted parameter for each subfault and visualized it. A similar resampling technique was successfully performed to visualize uncertainties in the 2011 Tohoku earthquake slip model (Hayes, 2011).

To understand the kinematics of an earthquake rupture, we calculated the effective rupture size and estimated the stress drop of the earthquake based on its inverted finite-fault rupture model. We followed the autocorrelation approach reported by Mai and Beroza (2000) to estimate the effective length (L_{eff}) and width (W_{eff}) of the rupture. The average static stress drop for each earthquake was computed by $\Delta\sigma =$

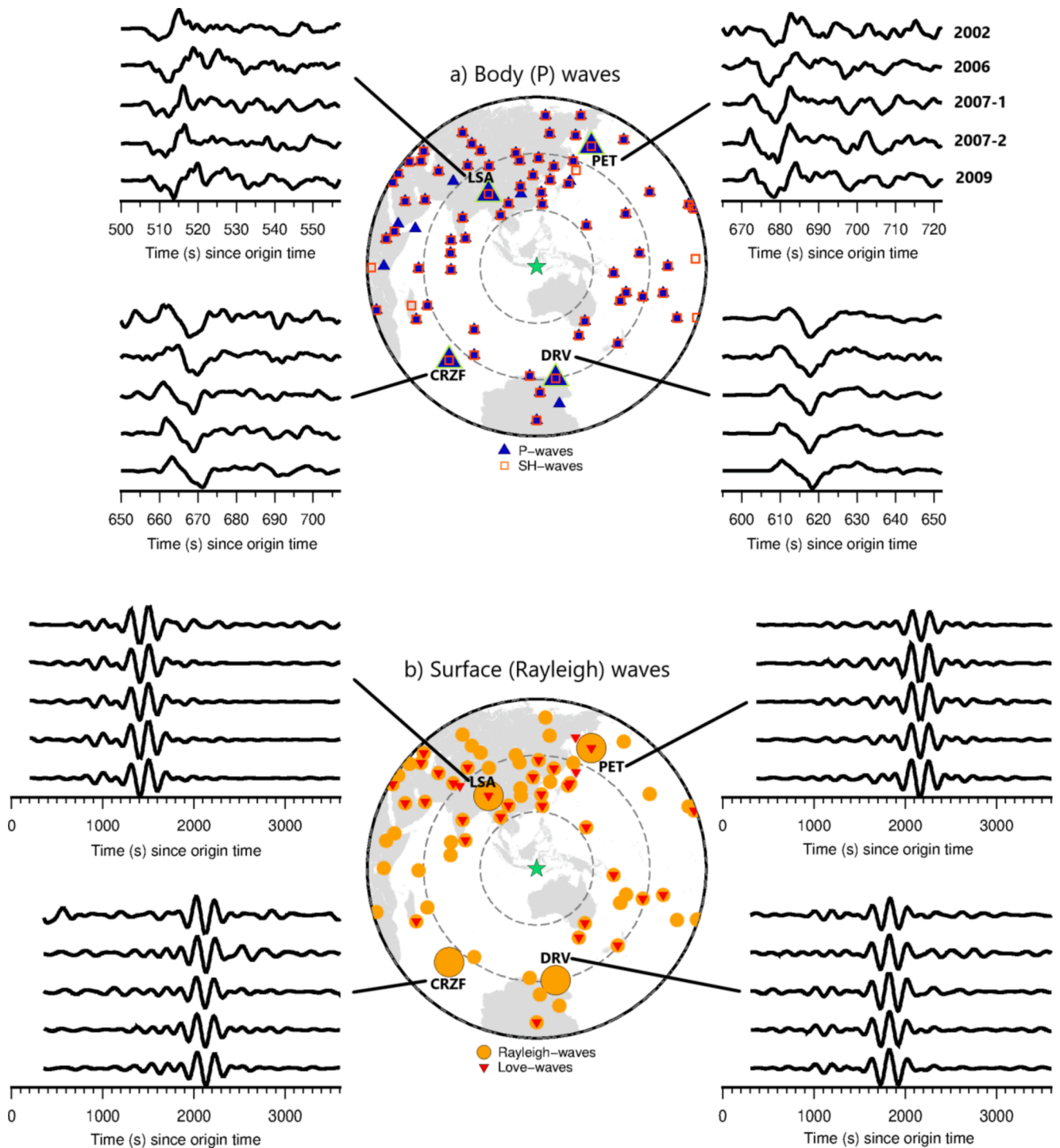


Fig. 2. Distributions of seismic stations and representative displacement seismograms (vertical components) of the 2002–2009 Sumbawa earthquakes at four selected stations (PET, DRV, CRZF, and LSA). (a) Body (P) waves and (b) surface (Rayleigh) waves. The star indicates the epicenter of the earthquake. Dashed circles represent the epicenter distance at a 30° interval.

$C \frac{M_0}{AL}$ (Kanamori and Anderson, 1975), where C is a nondimensional constant ($C = \frac{7\pi}{16}$ for a circular-shaped rupture; because initial results indicated circular-type rupture propagation for all events), M_0 is the inverted seismic moment, A is the effective fault area (A_{eff}), and L is the smaller characteristic length of the fault, either for the effective fault length or width (minimum of L_{eff} and W_{eff}) (Kanamori and Anderson, 1975).

4. Analysis and results

In this study, we successfully established the finite-fault rupture models and their STFs for the five earthquakes ($M_W = 6.2–6.6$) that occurred in Sumbawa. The stability and precision of the inversion results were evaluated by performing the jackknife resampling test. We plotted the subfaults with a standard deviation of $<20\%$, indicating higher precision. All waveform comparisons between observed and synthetic seismograms are available in the [supplementary data](#) and shown in

Figs. S1–S12. In general, our waveform inversions showed a satisfactory fit between observed and synthetic seismograms. However, we acknowledge few bad/noisy waveforms that showed not well-fitted waveform comparison, especially for the Love-waves (e.g., **Figs. S4, S6, and S8**). After a careful validation process, especially by removing these noisy seismograms, re-ran the inversion, we achieved consistent results with the present analysis (**Figs. S15–S22**). The use and display of those few noisy long-period seismograms are willing to provide more observation data examples for favorable azimuthally spatial coverage. The location of seismic stations with that few noisy long-period seismograms did not reflect representation from certain azimuths or distances; they were general long-period noises. In addition, we estimated the effective rupture size and the static stress drop of each individual earthquake. In this section, we present the large and complex rupture process event first (the 2009 event) and explain detailed analysis procedures. Then, other events are discussed in the following sections.

4.1. 2009 Event

On November 8, 2009 at 19:41:43.70 UTC, an earthquake ($M_W = 6.6$) caused light-to-moderate damages. This earthquake was the largest event and the most well-resolved of the 2002–2009 Sumbawa earthquakes. We set the rupture to initiate from the ISC-EHB epicenter (8.343°S, 118.618°E). According to ISC-EHB and USGS, the hypocenter depth of this earthquake was 21 and 18 km, respectively; however, the findings of our grid-search approach suggested that the rupture was best inverted from a depth of 15 km. We built a rectangular fault plane of this event with a strike of 90° (to the east) and a dip of 25° southward based on the global CMT double-couple solution. The final size of the fault plane used in the inversion was $20 \times 25 \text{ km}^2$, divided into 80 subfaults with a grid size of $2.5 \times 2.5 \text{ km}^2$. We inverted this earthquake by using 61 well-distributed broadband seismic stations containing 49P-wave, 45 SH-wave, 39 Rayleigh-wave, and 17 Love-wave seismograms. The

displacement seismograms of each body wave were 50 s in length from the first arrival, with a time interval of 0.2 s. The long-period surface waves had a length of 1 h (3600 s) from the origin time, with a time interval of 4 s. For a typical of moderate-magnitude events analyzed in this study, we used the same epicentral distance ranges (30°–90°) of the teleseismic stations for both the P and SH waves (e.g., **Hao et al., 2013; Twardzik and Ji, 2015**) with 50 s of time windows. At these ranges, we have used the direct P and SH waveforms to constrain the finite-fault rupture model and avoid the later arrivals, such as the PP and SS phases in the time windows for the finite fault inversion.

We transformed these seismograms into wavelet domains and minimized the difference (objective function) between the wavelet coefficients of observed and synthetic seismograms (**Ji et al., 2002**). Furthermore, we performed the simulated annealing method to determine the global optimal solution to describe each of the five unknown parameters (slip amplitude, rake angle, rupture initiation time, and starting and ending times of the normalized slip rate function) for each subfault. Finally, the synthetic seismograms showed a favorable agreement with the observed seismograms with a minimum cumulative misfit (objective function) of 0.209. We obtained the finite-fault rupture model, which included both the spatial and temporal slip evolution of each subfault.

After retrieval from the finite-fault rupture model, we visualized the STF (describing the rate of moment release with time after earthquake origin) and the subfault slip distribution (**Fig. 3**). The total inverted seismic moment was $9.74 \times 10^{18} \text{ Nm}$. This seismic moment was equal to an M_W of 6.6 following **Hanks and Kanamori (1979)** and similar to the moment magnitude of global CMT. After inversion, we observed that the rupture was initiated from the middle crust near 15 km (**Fig. 3d**). The peak slip (142 cm) was located at a deeper depth (17 km). The average slip was approximately 67 cm. The STF indicated rough progression with a total duration of approximately 12 s; however, the primary moment release occurred in the first 7 s. The jackknife test evaluated the

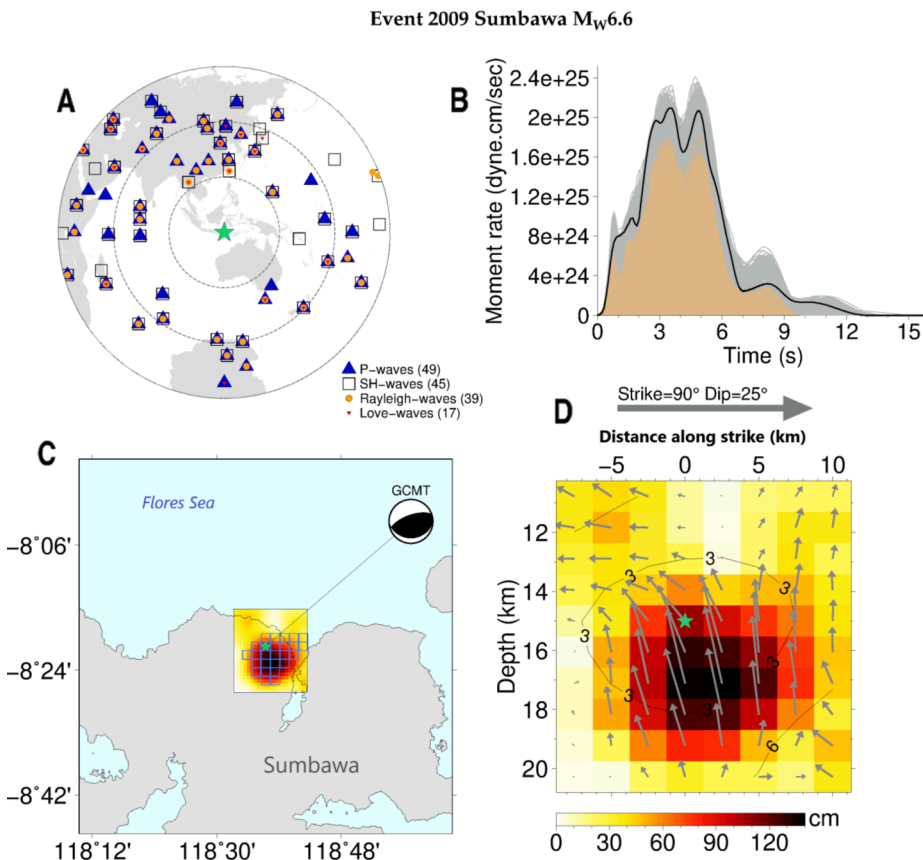


Fig. 3. Finite-fault rupture model for the 2009 event ($M_W = 6.6$) and its uncertainties. (a) Distribution of the teleseismic stations used in the inversion. Different symbols indicate different data types (i.e., P, SH, Rayleigh, and Love waves). The star indicates the epicenter of the earthquake. Dashed circles represent the epicenter distance at a 30° interval. (b) Moment rate function (MRF). The solid black line and brown-filled area show the final MRF solution based on all teleseismic data. The solid gray area indicates the MRF from each jackknife solution (150 individual inversions). (c) Surface projection of the slip distribution superimposed with the fault cell where estimated uncertainty (standard deviation) is lower than 20% of the subfault slip. Beachball shows a double-couple focal mechanism from the global CMT solution. The star is the epicenter of the earthquake. (d) Rupture process of the earthquake. The star is the hypocenter. Contours show the rupture propagation front at 3-s intervals. Gray arrows indicate the rake direction in each subfault. The large gray arrows indicate the strike direction.

uncertainties and demonstrated the robustness of our model, indicating that our moment rate function and most of the high slip subfaults were well resolved and had a high precision with a standard deviation (σ) of <20% (Fig. 3b and 3c). This earthquake had a single, compact, circular-shaped asperity with a thrusting mechanism at a depth of 14–20 km.

After retrieval from the finite-fault rupture model, we plotted the common time-slip amplitudes of each subfault on the fault plane and obtained the snapshot of the source rupture process. The snapshots collected at different time steps are used to present the propagation of fault rupture in Fig. 4. As shown in Fig. 4, the slip movement was dominated by the down-dip and along-strike directions. In this inversion, the rupture speed was not constant; however, we set it between 1.25 and 3.75 km/s following the procedure of Shao et al. (2011). We retrieved the inverted rupture initiation times for subfaults with a slip of >10 cm and used them to delineate the rupture speeds over the fault area. For this 2009 event, the down-dip rupture propagation was determined to have a speed of approximately 2.5 km/s but an up-dip propagation of only 1.7 km/s. The along-strike rupture movement had a speed of approximately 2.4 km/s. We followed the procedure and

approach reported by Mai and Beroza (2000) and estimated the effective length (L_{eff}) and width (W_{eff}) of the rupture (Fig. 5) as approximately 17.9 and 20.5 km, respectively. The average static stress drop estimated following the formula described by Kanamori and Anderson (1975) was approximately 2.0 MPa. Using the same procedure as that adopted to examine this 2009 event, we analyzed other earthquakes, namely the 2002, 2006, 2007–1, and 2007–2 Sumbawa earthquakes; the results are summarized in Table 1.

4.2. 2002 Event

This event occurred on October 6, 2002 at 15:46 UTC ($M_W = 6.2$). The total inverted seismic moment for this earthquake was 2.45×10^{18} Nm ($M_W = 6.2$) (Hanks and Kanamori, 1979). The rupture was initiated from a depth of 14 km with a peak slip of approximately 56 cm (Fig. 6). The rupture exhibited along-strike propagation in an eastward direction. The average slip of this event was approximately 27 cm. This earthquake had a single, circular-shaped asperity. The slip vectors indicated a thrusting mechanism. The STF of this earthquake had a simple, triangle

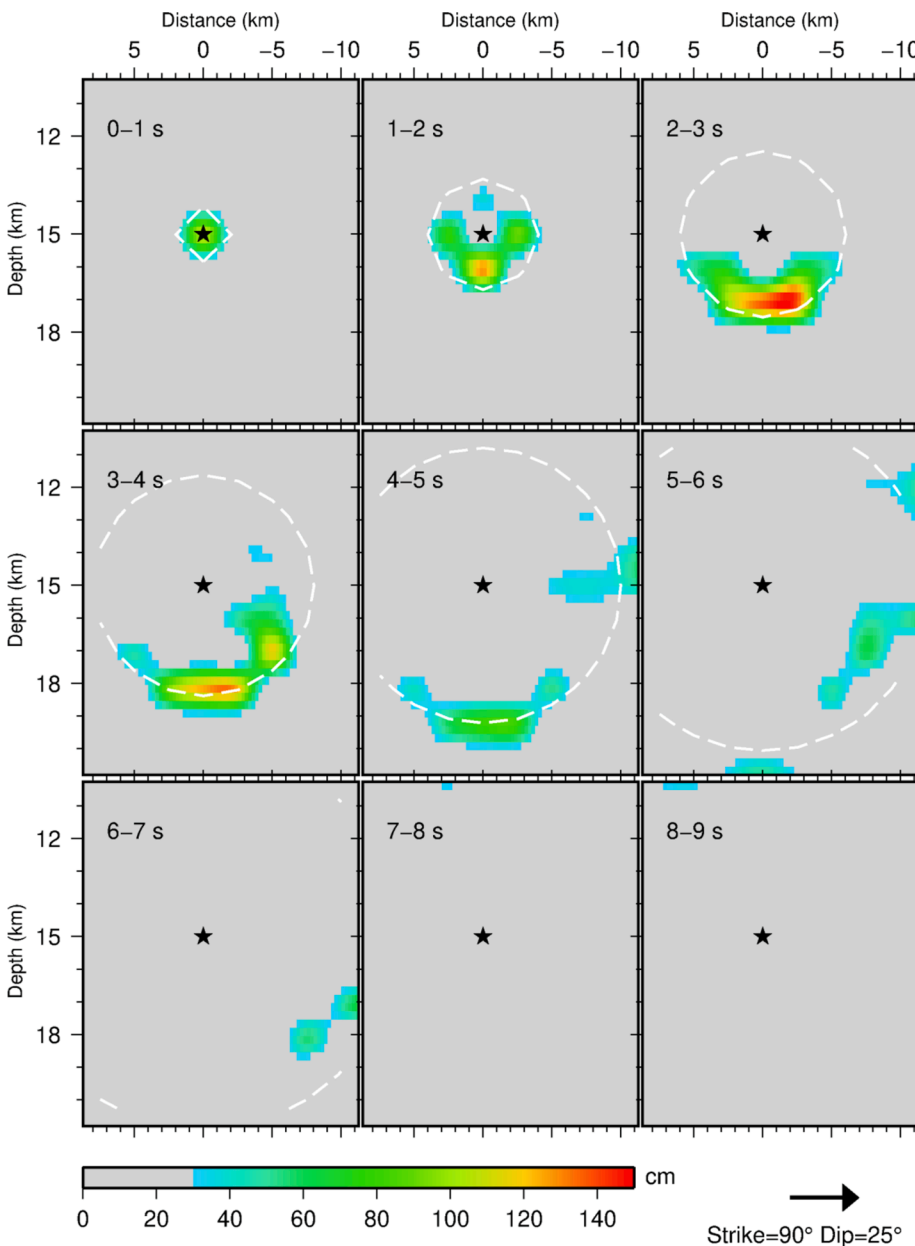


Fig. 4. Snapshots of rupture propagation of the 2009 event ($M_W = 6.6$). Each panel depicts the rupture propagation at 1-s intervals. Black stars represent the initial break of the rupture (i.e., the hypocenter). Color represents the slip amplitude at each time window. The dashed white lines indicate theoretical rupture time, assuming a rupture velocity of 2.0 km/s. The strike and dip information of the plane is available in the lower right figure. The slip is limited to an amplitude of >30 cm for plotting purposes.

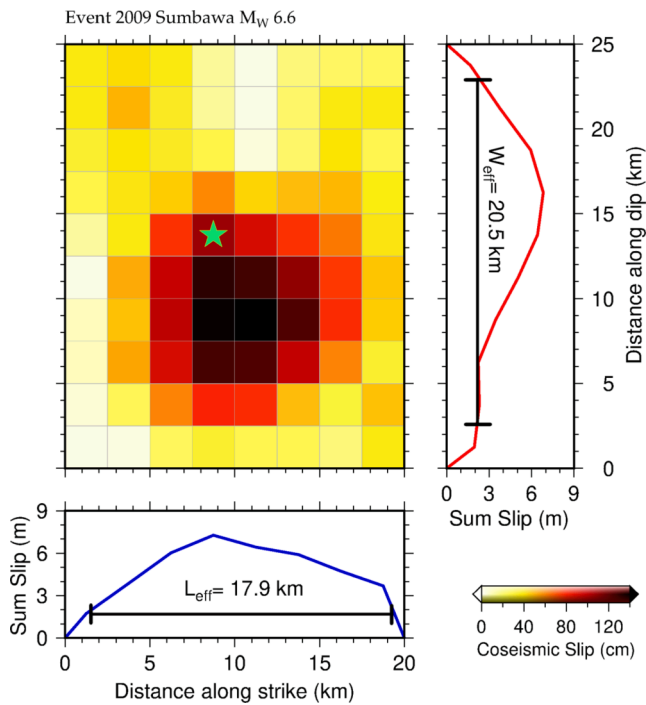


Fig. 5. Example of the estimation of the effective rupture dimension by using the method reported by Mai and Beroza (2000). The solid red and blue lines indicate the sums of slip amplitudes in the down-dip and strike directions, respectively. The solid black lines denote the effective length and width estimates from the autocorrelation method.

shape, with a rupture duration of 7 s. The average rupture speed was approximately 2.5 km/s. The effective length and width of the rupture were approximately 16.6 and 13.9 km, respectively. The static stress drop was approximately 1.0 MPa.

4.3. 2006 Event

This event occurred on December 1, 2006 at 14:01 UTC ($M_W = 6.3$) and caused light-to-moderate damage. It was the most eastern of the 2002–2009 sequence. The total inverted seismic moment was 3.6×10^{18} Nm ($M_W = 6.3$) (Hanks and Kanamori, 1979). The rupture of this event was initiated from a depth of 17 km (Fig. 7). The slip vectors showed a thrusting mechanism. The peak slip was approximately 55 cm, located nearly 5 km east of the initial break. The average slip was approximately 29 cm. This event had a single asperity with a circular shape. The effective size of the rupture was approximately 20.8×15.0 km, with an average static stress drop of nearly 1.1 MPa. The rupture snapshots presented a type of circular propagation with dominant along-strike propagation in an eastward direction (Fig. 8). The rupture stopped after a 10-s extension with average rupture speeds of approximately 2.5, 2.0, and 1.8 km/s for along-strike, down-dip, and up-dip propagation, respectively.

4.4. 2007–1 Event

On November 25, 2007, at 16:02 and 19:53 UTC, two earthquakes with $M_W = 6.5$ occurred with some moderate damages and six casualties. Both earthquakes were separated by only approximately 4 h. The first event had an inverted seismic moment of 5.51×10^{18} Nm ($M_W = 6.4$) (Hanks and Kanamori, 1979), slightly lower than the global CMT seismic moment ($M_W = 6.5$). The rupture was initiated from a depth of 15 km and had a single asperity. The STF of this event showed a smooth

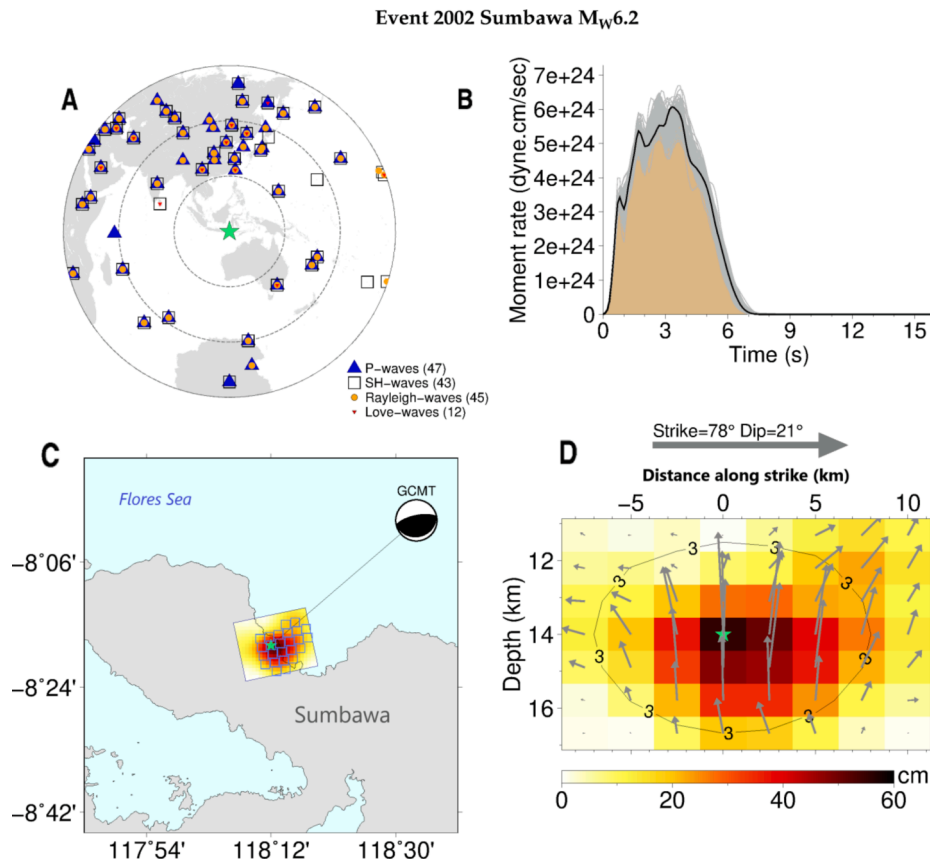


Fig. 6. Finite-fault rupture model for the 2002 event ($M_W = 6.2$) and its uncertainties. Other captions are similar to those for Fig. 3.

Event 2006 Sumbawa M_W 6.3

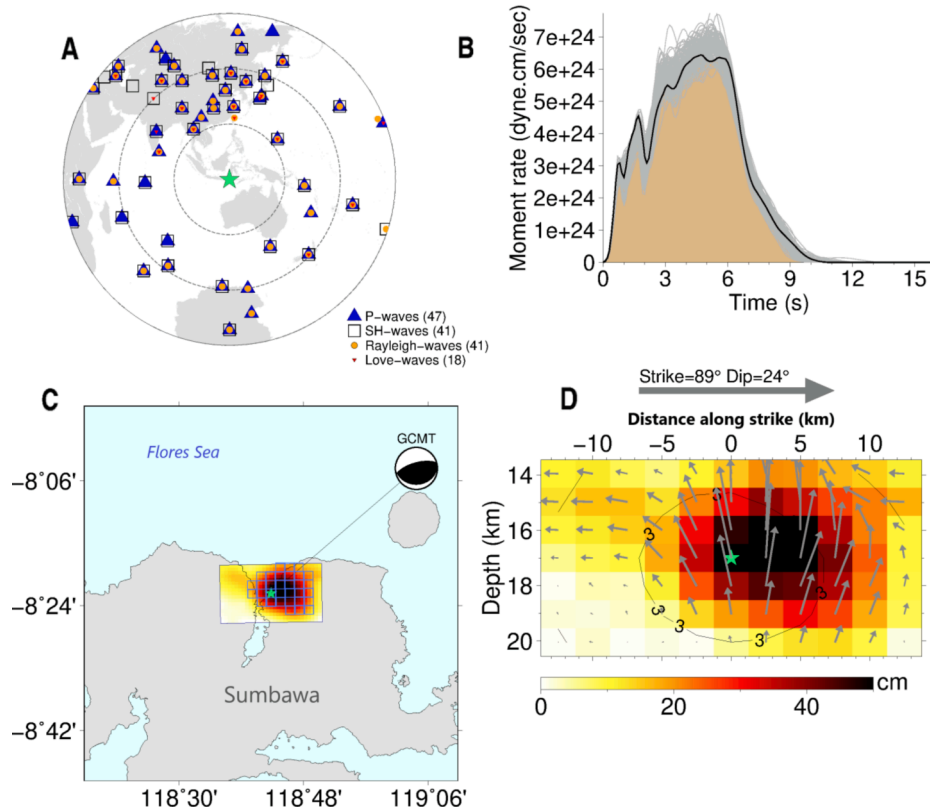


Fig. 7. Finite-fault rupture model for the 2006 event ($M_W = 6.3$) and its uncertainties. Other captions are similar to those for Fig. 3.

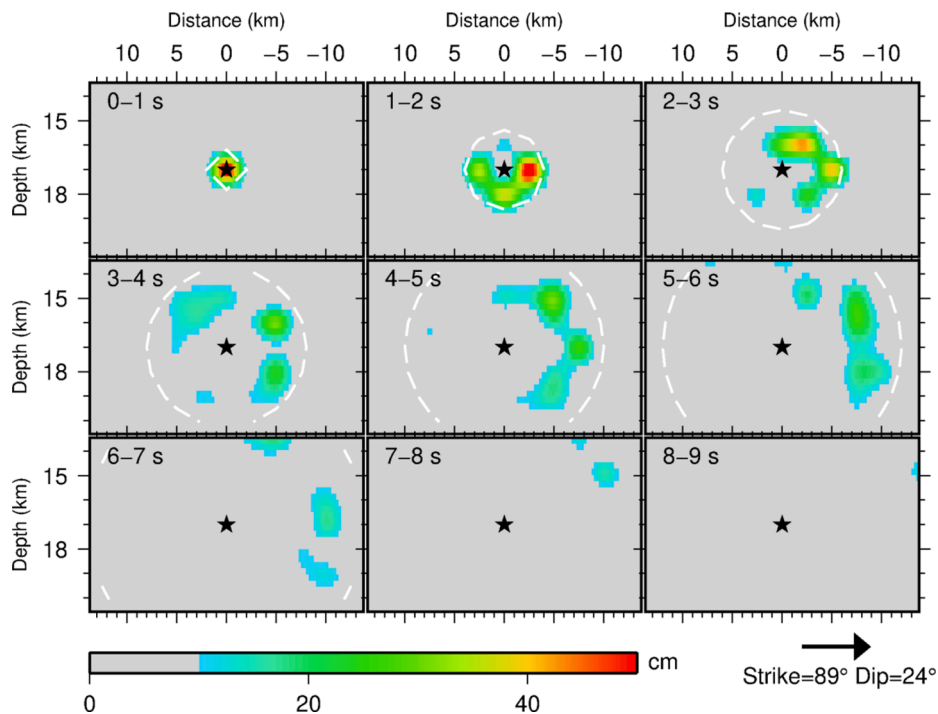


Fig. 8. Snapshots of the rupture propagation of the 2006 event ($M_W = 6.3$). Other captions are similar to those for Fig. 4. Here the slip is limited to an amplitude of >10 cm for plotting purposes.

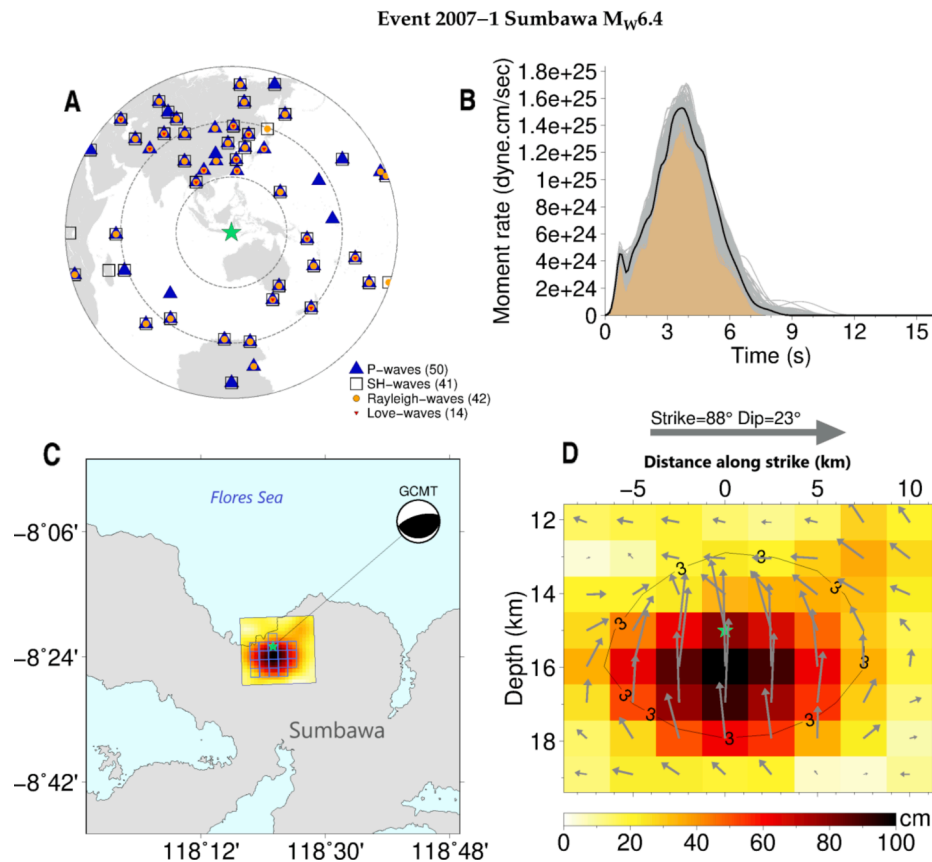


Fig. 9. Finite-fault rupture model for the 2007–1 event ($M_w = 6.4$) and its uncertainties. Other captions are similar to those for Fig. 3.

progression and was triangular in shape, with a duration of 8 s (Fig. 9). Most of the slip vectors depicted the thrusting mechanism. The peak slip was 105 cm at a slightly deeper depth (16 km). The average slip was approximately 47 cm. The effective length and width of the rupture were approximately 17.8 and 16.4 km, respectively. The static stress drop was approximately 1.6 MPa. The rupture was dominated by down-dip propagation. Down-dip, up-dip, and along-strike rupture propagation had speeds of approximately 2.5 km/s, 1.7, and 2.4 km/s, respectively.

4.5. 2007–2 Event

This second event occurred just approximately 4 h after the 2007–1 event. The total inverted seismic moment for this earthquake was 5.72×10^{18} Nm ($M_w = 6.4$) (Hanks and Kanamori, 1979). The STF indicated that this earthquake had a rougher moment release than the preceding earthquake. This event was initiated from a depth of 12 km, and the rupture finished after a duration of 11 s (Fig. 10). The peak slip was approximately 73 cm, much smaller than that of the 2007–1 event. The well-resolved slip distribution indicated a circular-shaped rupture with a single asperity. The average slip was approximately 32 cm. The effective rupture size was approximately 21.7×23.5 km with an average static stress drop of approximately 0.7 MPa. The earthquake was dominated by down-dip propagation with a speed of approximately 2.2 km/s.

4.6. Validation by empirical green's function analysis

We used Empirical Green's Functions (EGF) analysis to validate our source-parameter result using higher-frequency seismograms. We used 40 s of unfiltered seismograms (5 s before to 35 s after P-wave arrival) to perform deconvolution of the EGF waveforms for the 2006, 2007–1, 2007–2, and 2009 events (data for the 2002 event were unavailable). We chose two smaller events ($M_w = 5.3$ and 5.4, respectively) as our EGFs

located very close to the 2002–2009 events and observed their focal mechanisms, which were similar to 2002–2009 events. We performed the EGF analysis using the multitaper method (Prieto et al., 2009; Abercrombie, 2015). As seen from station KAPI located northeast of the cluster, the results indicated that the duration and general shapes of the moment rates of apparent STF determined from EGF analysis were consistent with the results of the finite-fault inversion (Fig. 11).

5. Discussion

In this study, we obtained the detailed source parameters and rupture characteristics of five earthquakes that occurred from 2002 to 2009 in the Sumbawa segment of Flores Thrust. The results showed similarities in the rupture processes and cascading asperities by neighbor fault patches. We further discuss detailed rupture behaviors, namely rupture initiation, rupture speed, rupture size, and stress drop, and compare them with those of other global and regional earthquakes. In addition, we highlight the implications of our study findings for future seismic and tsunami hazards, particularly for Sumbawa Island.

5.1. Rupture initiation

In general, all ruptures during the 2002–2009 sequence were nucleated in the middle crust (at a depth of approximately 12–17 km). These initiation depths were shallower than the hypocenter depths suggested by the ISC-EHB catalog (14–27 km) (Engdahl et al., 2020); however, they were still within the uncertainty range of their 10-km depth resolution (Engdahl et al., 2020). The hypocenter depths of the five earthquakes vary substantially between agencies (e.g., USGS and ISC-EHB). However, using the grid-search procedure that obtains the best waveform fits, we observed that they were generally at similar depths (Fig. 12). We conducted several models tests to confirm that

Event 2007-2 Sumbawa M_w 6.4

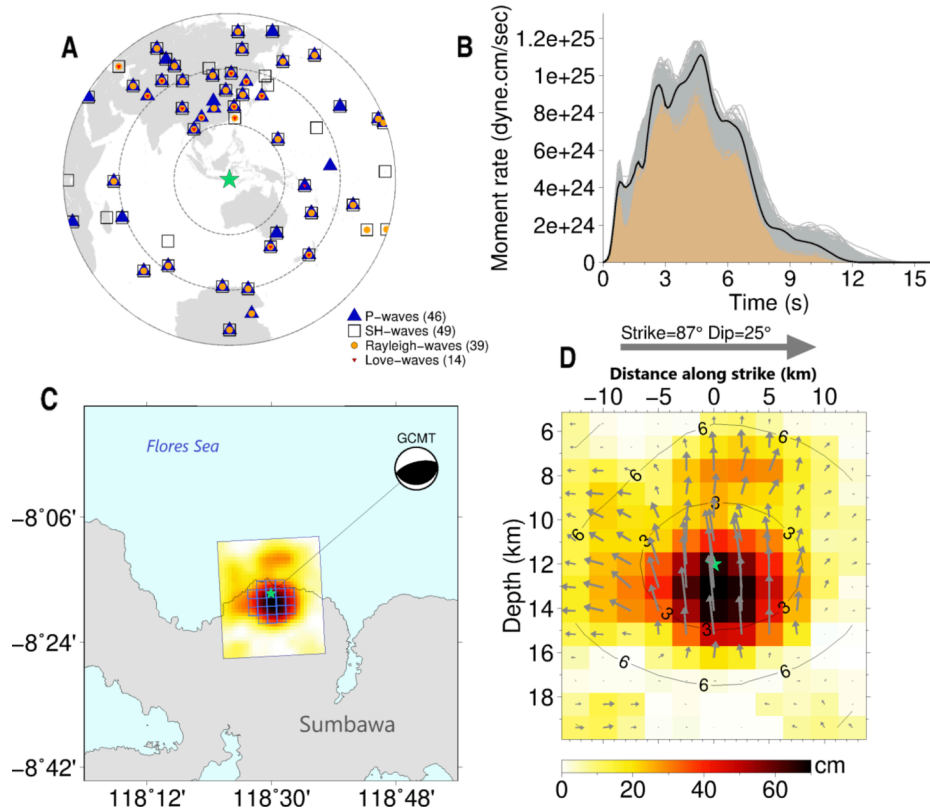


Fig. 10. Finite-fault rupture model for the 2007-2 event ($M_w = 6.4$) and its uncertainties. Other captions are similar to those for Fig. 3.

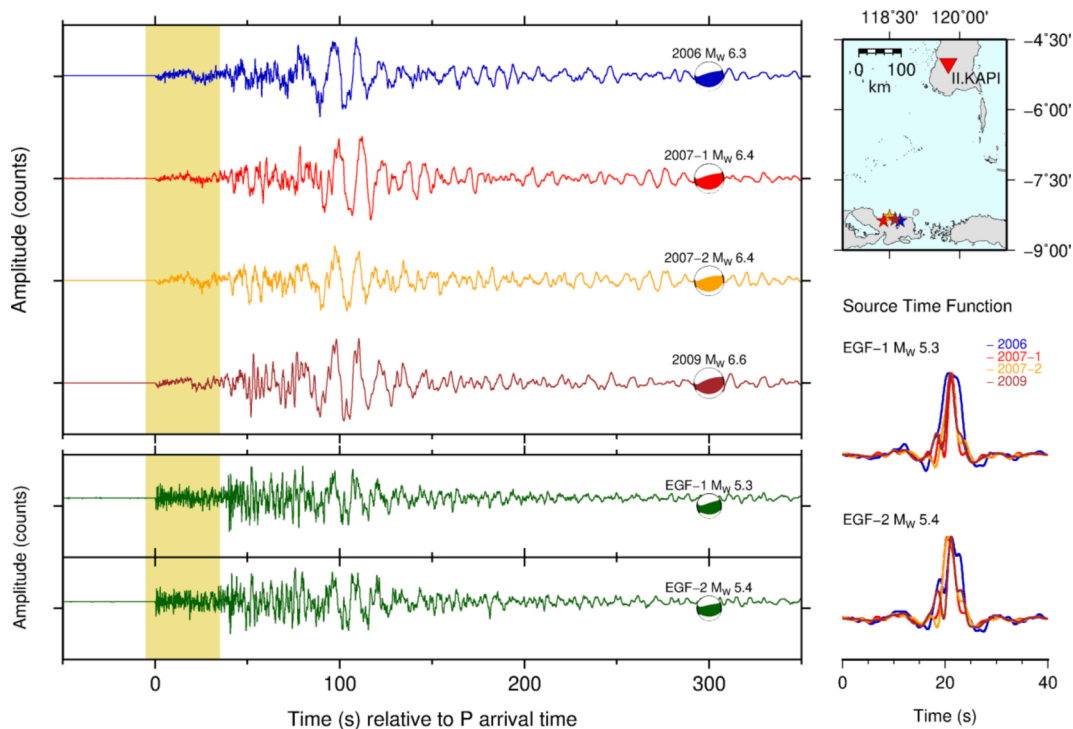


Fig. 11. Relative STFs at station II KAPI computed using the EGF method. EGFs were obtained for the 2007-11-26 08:15 UTC ($M_w = 5.3$) and 02:32 UTC ($M_w = 5.4$) events, with locations identical to those of the five Sumbawa earthquakes. The yellow dashed colors show the P-wave time window used in the EGF method. Beachballs at the ends of the seismograms are double-couple focal mechanisms from global CMT. The focal mechanisms of the EGFs are similar to those of the larger earthquakes analyzed in this study. The map shows the location of the II KAPI station relative to the epicenters of the earthquakes. The relative normalized STFs obtained from the II KAPI station are shown in the bottom right.

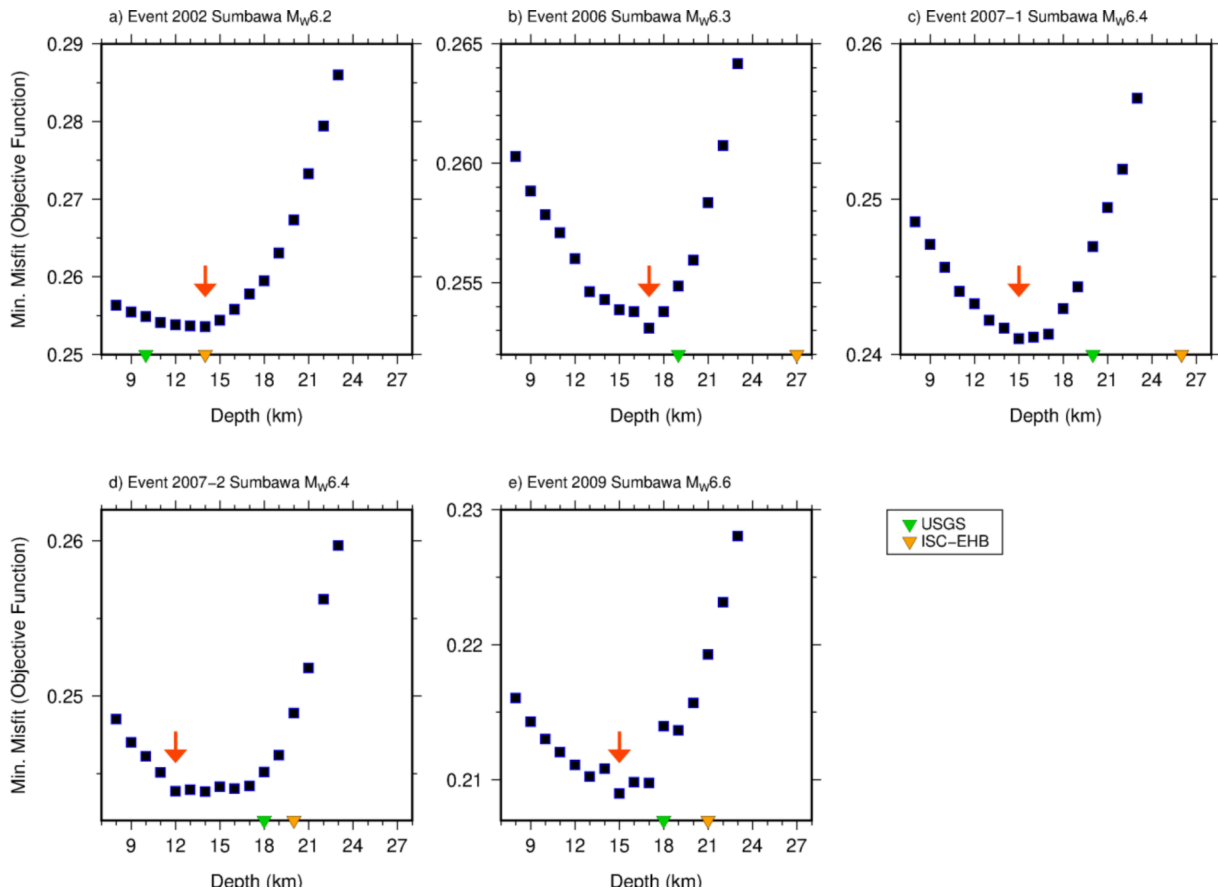


Fig. 12. Grid search for optimal initiation depths for each earthquake (a-e). The black squares indicate the waveform misfit by using the individual initiation depth. The arrows indicate the optimal rupture initiation depth. Green and orange inverted triangles depict the USGS and ISC-EHB hypocenter depths, respectively.

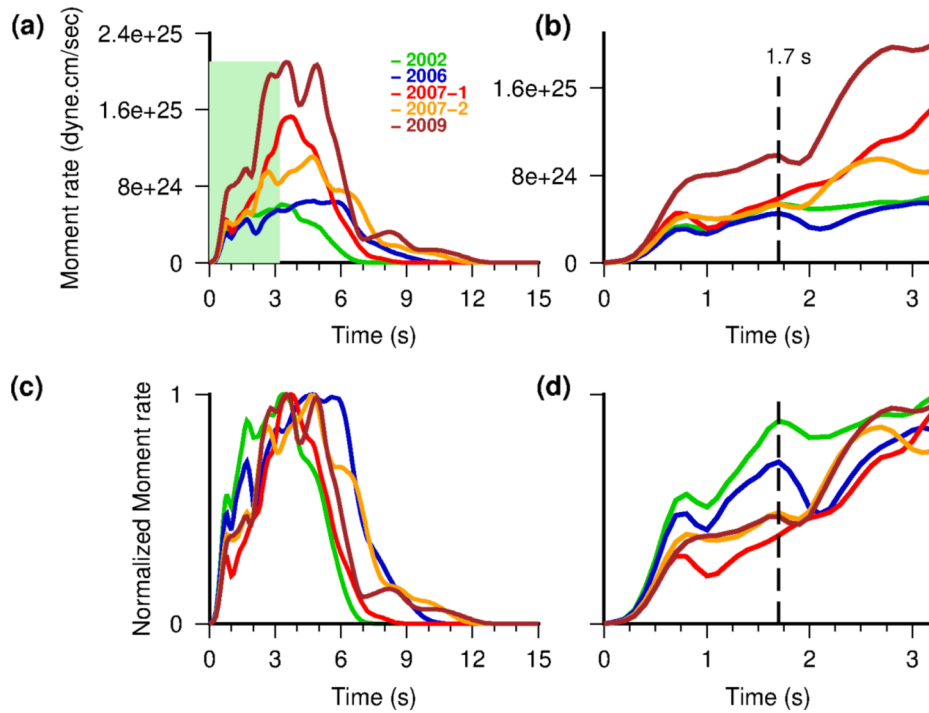


Fig. 13. (a) Average STFs for 2002–2009 Sumbawa earthquakes from finite-fault inversions represented by different colors. The green dashed area is the time window for Fig. 13b. (b) Enlarged STFs for the first 3.2 s showing the rupture initiation part. (c) Normalized (relative) STFs. (d) Normalized STFs for the first 3.2 s. Black dashed line is a time marker for 1.7 s.

using different seismic crustal velocity models around the source region did not change the initiation depth of the ruptures. Those seismic velocity models and corresponding test results can be found in Figs. S13–S14.

The STF_s indicated that the rupture initiation shapes were similar in approximately the first 1.7 s for all the earthquakes (Fig. 13), as shown by their comparable early-stage slopes (Colombelli et al. 2020; Melgar and Hayes, 2019). The rupture initiation shapes were nearly identical for the 2002, 2006, 2007–1, 2007–2 Sumbawa earthquakes, with M_W ranging from 6.2 to 6.4, and comparable to the 2009 earthquake, which had an M_W of 6.6 (Fig. 13b and 13d). This result is consistent with the conceptual STF_s model proposed by Colombelli et al. (2020) for ruptures with comparable nucleation slopes. In this model, the initial slope of STF_s increased with magnitude. Teleseismic inversions generally exhibited an excellent temporal resolution, as demonstrated by these STF_s, indicating the reliability of this result. Moreover, the consistency and resolution of this result were tested using the jackknife resampling test (Fig. 3c).

From the EGF analysis performed using data from the KAPI station, the rupture initiation shapes, as suggested by this study, were clarified and more evident. Apparent STF_s determined from EGF analysis at KAPI showed an initial moment release of approximately 2 s (Fig. 11), comparable with average STF_s obtained from finite-fault inversions. We also compared our results with STF_s obtained from the SCARDEC database (Vallée and Douet, 2016), which collected source parameters for global moderate-to-large earthquakes by using very-low-frequency body waves. The STF_s of events analyzed in this study showed similar rupture initiations, durations, and relative maximum slip peaks, which were processed based on different seismic signal frequency bands.

This rupture initiation might indicate that they required identical stress conditions and preparatory growth processes to generate the dynamic rupture (Ellsworth and Beroza, 1995). Since only five earthquakes were analyzed in this study, the possibility of the comparable earthquake initiation phases along the Flores Thrust fault needs to verify continuously. Earlier studies indicated that the beginning of rupture signals could estimate the final earthquake size and thus be helpful for future earthquake early warnings (Colombelli et al., 2020; Melgar and Hayes, 2019; Meier et al., 2021).

5.2. Rupture speed

According to the assumption of the inversion method used in this study (Ji et al., 2002; 2003; Liu and Yao, 2018; Shao et al., 2011), the

rupture speed was not constant; however, we set it to be between 1.25 and 3.75 km/s. The inverted typical average rupture speed of the 2002–2009 Sumbawa earthquakes was approximately 2.0–2.5 km/s for along-strike and down-dip propagation (Fig. 14). This speed is consistent with the rupture speed of the thrusting rupture observed in some earthquakes (e.g., the 1999 Chi-Chi earthquake in Taiwan) (Huang, 2001). In addition, this speed is consistent with the rupture speed of the 1992 Flores Thrust earthquake ($M_W = 7.7$) estimated by a previous study (Pranantyo and Cummins, 2019). However, the rupture speed for up-dip propagation to a shallower depth was generally lower than that for along-strike and down-dip propagation by approximately 1.7 km/s (Fig. 14).

5.3. Rupture size and stress drop

In this study, effective rupture dimensions were computed using the method reported by Mai and Beroza (2000) that involved the use of the autocorrelation function of slip along-strike and dip propagation (Hayes, 2017). Some other studies have adopted different techniques to obtain the effective rupture size from finite-fault rupture models, for example, by removing subfaults with amplitudes smaller than a certain fraction of peak slips (Hao et al., 2013; Somerville et al., 1999; Ye et al., 2016). Following the procedure reported by Ye et al. (2016) to remove subfaults with a slip amplitude smaller than 17% of the peak slip, we obtained a comparable rupture size that was computed using the method proposed by Mai and Beroza (2000) (Table 1).

The rupture characteristics associated with the 2002–2009 Sumbawa earthquakes showed a low average static stress drop of approximately 1.0–2.0 MPa for all earthquakes, except the 2007–2 event, which showed a slightly lower stress drop (0.7 MPa; Table 1 and Fig. 15). Using the seismic-spectra-based approach, Allmann and Shearer (2009) determined that both the 2002 and 2006 Sumbawa events had a stress drop of 1.7 MPa. These findings indicated the consistency of both approaches. A typical stress drop of 1.0–2.0 MPa was notably lower than the global average stress drop. The global seismic-spectra-based computation suggested that the stress drop of individual earthquakes ranged from 0.1 to 100 MPa, with a median of approximately 3.0–4.0 MPa (Allmann and Shearer, 2009; Neely et al., 2020). The median stress drop of global subduction thrust earthquakes and the continental collision zone were approximately 2.0–3.0 and 2.6 MPa, respectively, and thrust faulting had a lower stress drop than strike-slip earthquakes (Allmann and Shearer, 2009). In addition, the global finite-fault-based stress drop estimates (Ye et al., 2016) suggested an average stress drop

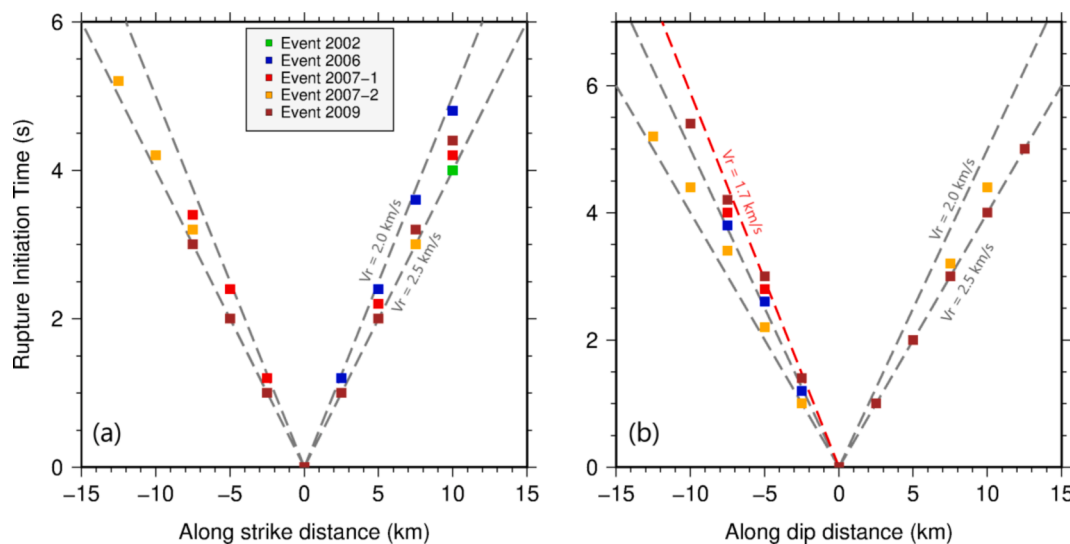


Fig. 14. Rupture speed for (a) along-strike distance and (b) along-dip distance. The speed was plotted from subfaults with a slip amplitude of >10 cm (see Figs. 4 and 8).

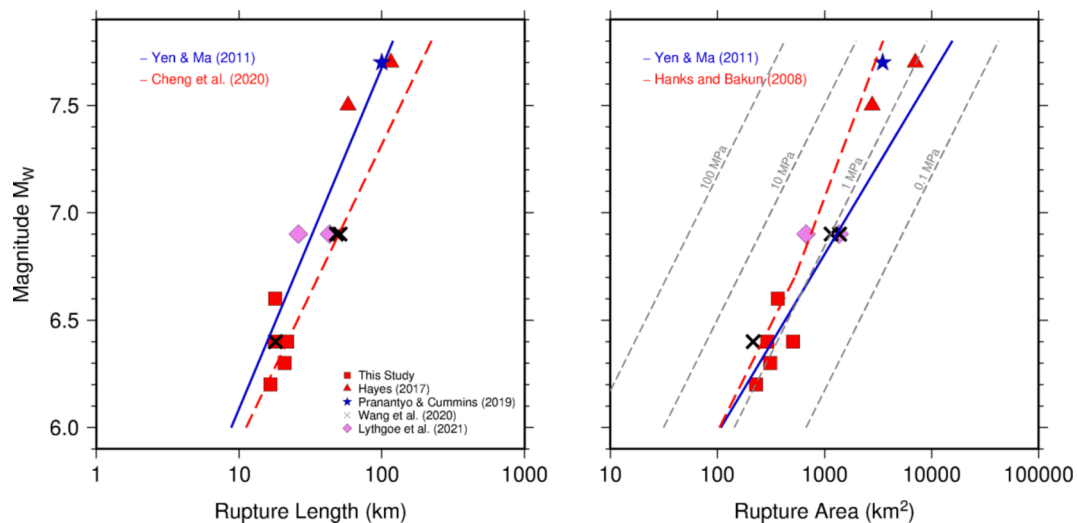


Fig. 15. Comparison of the rupture dimensions of 2002–2009 Sumbawa earthquakes with other earthquakes ($M_W > 6$) since 1990 along the Flores Thrust (Hayes, 2017; Lythgoe et al., 2021; Pranantyo and Cummins, 2019; Wang et al., 2020) based on published earthquake source scaling (Cheng et al., 2020; Hanks and Bakun, 2008; Yen and Ma, 2011).

of approximately 3.0–4.0 MPa.

The relatively low stress drop of the 2002–2009 earthquake ruptures could be related to the properties of the Flores Thrust fault zone that may have occurred in the crust that was highly fractured and thus weaker (McCaffrey and Nábělek, 1987). Furthermore, the lower stress drop could be related to the crust condition with a more brittle characteristic that enables the easy release of strain accumulated by fractures (McCaffrey and Nábělek, 1987; Sharma and Wason, 1994; Taymaz et al., 2021). Indeed, the low stress drop could reflect the existence of magmatic fluids that resulted in the weakening of fault strength within western Flores Thrust (Silver et al., 1983). However, even though the 2002–2009 Sumbawa events were located close to the volcanic region (such as the Tambora volcano that exists west of the five asperities), the stress drop spatial distribution did not reflect the relations to this interpretation. Further appraisal of stress drop of more earthquakes in this region and seismic tomography imaging may answer this aspect in the near future. It is noteworthy that energy-based stress drop computation (Noda et al., 2013; Ye et al., 2013, 2016) may provide better constraints and can be applied to analyze source characteristics of Flores Thrust events.

5.4. Architecture of the Flores Thrust

The finite-fault rupture models provided in this study offer insights into the geometry and seismogenic depth of the Sumbawa segment of Flores Thrust as well as the distribution of asperities along western Flores Thrust. The strike direction and dip angle of the fault were obtained from the global CMT parameter (Ekström et al., 2012). For the five earthquakes, the strike orientations were indistinguishable (strike = 87° – 90°), except for the 2002 event with a strike of 78° . Their dip angles were the same for all earthquakes (dip = 21° – 25°). Our preliminary inversions suggested that the global CMT fault geometry fit much better than any other variations such as the detachment model of Flores Thrust (low dip, $\sim 13^\circ$) or possible higher-angle splay fault (moderate dip, $\sim 44^\circ$) (McCaffrey and Nábělek, 1984; Yang et al., 2020). These fault orientations are consistent with the geometry of the Flores Thrust in Lombok analyzed by previous studies; for example, a dip of approximately 25° was applied by Lythgoe et al. (2021). Yang et al. (2020) and Lythgoe et al. (2021) have analyzed marine seismic profiles to determine this fault dip. This dip angle of the Flores Thrust is also consistent with the 1992 Flores earthquake (Beckers and Lay, 1995; Pranantyo and Cummins, 2019).

On the basis of the findings of all inverted rupture models in this study, the seismogenic depths in the Flores Thrust during the 2002–2009 earthquakes ranged from approximately 10 to 20 km. This seismogenic width is consistent with Lombok earthquakes (in the west) inverted by previous studies (Lythgoe et al., 2021; Salman et al., 2020; Wang et al., 2020). An earlier geodetic study suggested that the segment north of Sumbawa had the deepest locked fault segment along the Flores Thrust (Koulali et al., 2016).

The 2002–2009 Sumbawa earthquakes ruptured fault patches in the east of Tambora volcano and appeared to be different from 2018 Lombok earthquakes (four earthquakes with $M_W > 6.0$) that occurred beneath Rinjani volcano on Lombok Island (Lythgoe et al. 2021). In comparison, the 2018 sequence had an energetic and unusual seismicity evolution (approximately 200 earthquakes with $M_L \geq 4$ within approximately 1 month), an observation that we did not find in the Sumbawa earthquakes. That Lombok sequence appeared to be strongly controlled by the volcano–earthquake interaction (Lythgoe et al., 2021; Afif et al., 2021).

The 2002 earthquake with $M_W = 6.2$ ruptured the westernmost patch of the 2002–2009 sequence, with the peak slip slightly higher than that of the 2006 earthquake ($M_W = 6.3$), which ruptured the easternmost patch. However, the asperity size estimate for the 2006 event was higher than that of the 2002 event. The two 2007 earthquakes ($M_W = 6.4$) ruptured to the east of the 2002 earthquake. A gap of approximately 10 km was noted between 2002 and 2007 rupture patches. The first 2007 earthquake ($M_W = 6.4$) had a larger slip amplitude and narrower rupture size (stress drop = 1.6 MPa) than its twin (stress drop = 0.7 MPa), which also had a shallower depth. The 2009 earthquake ($M_W = 6.6$) then ruptured east of the 2007 earthquakes and west of the 2006 rupture. The 2009 earthquake ruptured with a significantly large slip amplitude, leading to a higher stress drop (2.0 MPa). Each earthquake had a single squeeze asperity, similar to the two asperities of the Lombok earthquakes (Lythgoe et al., 2021; Salman et al., 2020; Wang et al., 2020).

Most of the recent seismicity (2009–2020) recorded by BMKG's permanent broadband seismic network occurred northwest and up-dip of the 2002–2009 earthquakes (Fig. 1c). This recent seismicity appeared to fill the westernmost part of a possibly shallower seismic gap, located up-dip of the 2002–2009 sequence. Some earthquakes also occurred in the northeast, probably located in the shallowest up-dip section (or “near trench”) of the Flores Thrust zone (Fig. 1c).

5.5. Two kinematic interpretations

We observed that the 2002–2009 earthquakes ruptured neighboring fault patches within approximately 8 years. The asperities did not overlap (Fig. 16). The ruptures were prevented from growing large in size, for example, into a single earthquake with $M_W > 7$. When we combined the lengths of all 2002–2009 earthquakes, we obtained a 77-km rupture length equivalent to a thrust earthquake with $M_W = 7.3$ based on the relationship reported by Wells and Coppersmith (1994). During seismological instrument periods (since ~ 1963), seismicity in the western Flores Thrust (from the north of Sumbawa to Lombok and Bali) indicated a consistent cascading behavior of earthquake ruptures (Wang et al., 2020). In addition to the 2002–2009 Sumbawa sequence investigated in the present study, the global earthquake catalog indicated the 1979 earthquake sequence north of Bali (Fig. 16 inset), which included three earthquakes ($M_W = 6.2$) within 7 months. More recently, the 2018 Lombok sequence (Fig. 16 inset) with a cascade of one $M_W=6.3$, one $M_W=6.4$, and two $M_W=6.9$ earthquakes ruptured north of Lombok Island within 3 weeks (Lythgoe et al. 2021; Wang et al., 2020). These cascading features of moderate-magnitude ruptures ($M_W = 6.2$ – 6.6)

might be related to fault immaturity (Perrin et al., 2016; Wang et al., 2020; Thakur and Huang, 2021; Manighetti et al., 2021). The typical low stress drop of the 2002–2009 Sumbawa events might also be an indication of fault immaturity (e.g., Thakur and Huang, 2021). The western Flores Thrust was initiated at approximately 3–5 Ma and is believed to be a less mature fault system (Hall, 2012; Wang et al., 2020). The eastern Flores Thrust was initiated during the early stage of the Flores Thrust and is more mature than the western Flores Thrust (Hall, 2012; McCaffrey and Nábělek, 1987). We did not observe these cascading features in the eastern Flores Thrust, which ruptured in a single large earthquake (the 1992 Flores earthquake; $M_W = 7.7$) (Beckers and Lay, 1995; Pranantyo and Cummins, 2019). Similarly, the Wetar Thrust—the back-arc thrusting fault east of the Flores Thrust—also ruptured in a large earthquake ($M_W = 7.5$) in 2004 (Fig. 1). However, this 2004 earthquake was poorly investigated (Hayes, 2017). As the first interpretation, the cascade earthquake cluster with M_W ranging from 6.2 to 6.6 during the 2002–2009 Sumbawa sequence implied that fault segments prohibited the growth of a single large earthquake ($M_W > 7$) or that significant structural controls existed for the rupture extent (e.g., Salman et al., 2020).

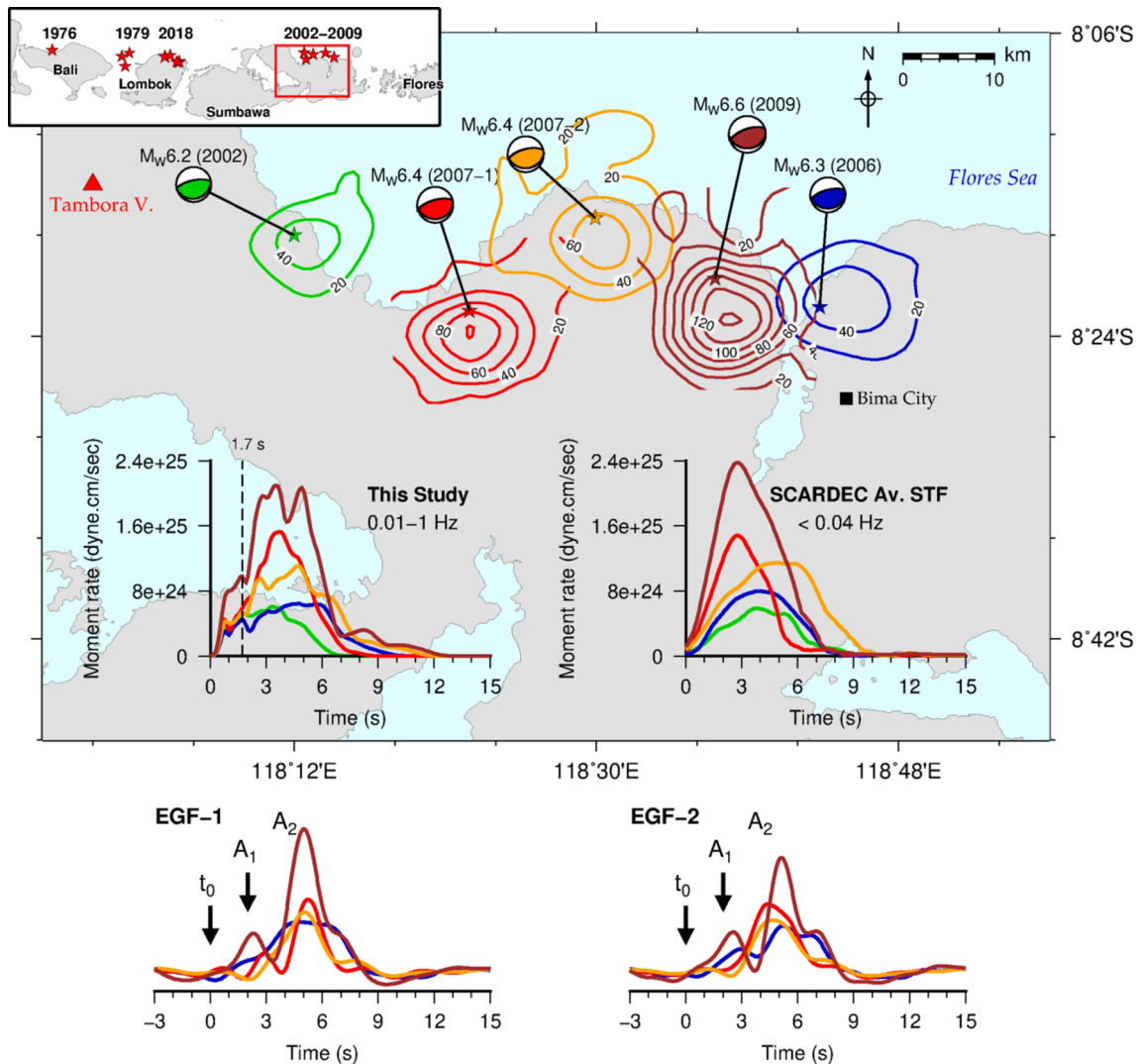


Fig. 16. Asperity locations and STF during 2002–2009 Sumbawa earthquakes. Contours depict the fault ruptures inverted in this study, and stars depict their epicenters. Different colors represent different earthquake ruptures with slip amplitudes of >20 cm and intervals of 20 cm. The red triangle indicates the location of the Tambora volcano. The lower left panel shows the MRFs for the five earthquakes in this study. The relative STF obtained using the EGF method, as seen from the II KAPI station (Fig. 11), are shown below. A_1 denotes the distinctive moment release of the rupture initiation phase, A_2 is the primary moment release, and t_0 indicates the interpreted first break of the rupture. For comparison, the very-low-frequency STF obtained from the SCARDEC database are shown (Vallée and Douet, 2016). The inset figure shows the epicenters of shallow earthquakes ($M_W > 6$) during the instrumental period.

An alternative (second) interpretation is that the western Flores Thrust is as mature as the eastern parts; however, the cascade features of earthquakes with M_W of 6.2–6.6 represent asperities near the down-dip brittle-ductile transition (Lay et al., 2012). These smaller asperities that nucleated from the middle crust (e.g., the deeper part of the fault) showed a difference of along-dip fault mechanics in shallower patches that have not yet ruptured (Lay et al., 2012) (Figs. 1 and 17). These earthquakes reflect a heterogeneous state of stress and strength on the fault between the deeper part that ruptured with multiple asperities and the shallower part or “near trench” (e.g., down-dip segmentation), which can be treated as a seismic gap (Fig. 1c and 17). This behavior was observed for the subduction zone megathrust earthquakes (Lay et al., 2012; Nishikawa et al., 2019). Fuchs et al. (2014) indicated that the Sumbawa segment of the Flores Thrust may have nonvolcanic tremors at a deeper depth, which is similar to the slow-earthquake features observed in subduction zone thrust faults (Nishikawa et al., 2019).

5.6. Possible seismic gap

As discussed above, the regional earthquake catalog (BMKG network, 2009–2020) indicated a possible seismic gap north of the 2002–2009 asperities (Fig. 1). In addition, the finite-fault rupture models of the 2002–2009 earthquakes also suggested asperities interaction and down-dip segmentation of the Sumbawa segment of Flores Thrust, which also indicated a possible seismic gap in the up-dip part. Thus, the subsequent analysis of these five earthquakes provides insights into the seismic rupture process and future seismic hazards in the Sumbawa region.

Areas of high slip for the five events do not overlap, suggesting an adjoining pattern of asperity zones consistent with prior observations in the 2018 Lombok earthquakes. We observed that the down-dip and along-strike rupture propagations are more abundant than up-dip ruptures (e.g., Figs. 4, 8, and 14), which can be understood as a consequence of the material contrast. A frictionally locked large shallow asperity in Sumbawa (the seismic gap) might be surrounded by deep but smaller asperities with different frictional properties (Fig. 17) (Lay et al., 2012; Nishikawa et al., 2019). This interpretation implies that future earthquakes originating in the shallower seismic gap of the Sumbawa segment have potential magnitudes of >7.0 based on the combined

length of smaller asperities in 2002–2009. Some studies outlined that the shallowest parts of the thrust fault zone are also capable of large coseismic slip, such as in the 1999 Chi-Chi (Taiwan) earthquake (e.g., Hubbard et al., 2015). It is also worth noting that, in comparison, for the large Flores thrust earthquakes, such as the 1992 M_W 7.7 Flores earthquake and the 2004 M_W 7.5 Wetar Thrust earthquake, the rupture nucleated from the middle crust and propagated dominantly up-dip to the shallowest part of the Flores Thrust fault (Hayes, 2017); the similar situation could happen in Sumbawa.

Indeed, historically, an earthquake with $M_W > 7.0$ occurred in Sumbawa in 1836; however, the exact location and precise magnitude was unknown (Koulali et al., 2016; Musson, 2012; Pranantyo et al., 2021; Griffin et al., 2019). As shown in Fig. 15, a rupture with $M_W > 7.0$ could have a rupture length of at least 40 km, comparable with the size of the shallow seismic gap shown in Fig. 1. This shallow rupture could generate significant ground motion and a tsunami. Because earthquakes with a lower stress drop tend to radiate less high-frequency ground motion (Hao et al., 2013; Somerville et al., 1999), the damage caused by future large Sumbawa earthquakes might be due to shallow rupture nature and probable hanging wall effects. In addition, our source analysis, including the stress drop and rupture velocities, has implications for assessing the peak ground acceleration (PGA) variability for the Sumbawa region (Chounet et al., 2018). Given the high seismic and tsunami threat in Sumbawa Island, hazard analysis in this region is urgently required for earthquake engineering applications.

5.7. Implications for regional seismic and tsunami hazards

The 2002–2009 Sumbawa earthquakes resulted in considerable hazards. The 2006 event was felt in Bima city with a Modified Mercalli Intensity (MMI) of V. The two 2007 events ($M_W = 6.4$) occurred on the same day and caused moderate damage. The 2009 event ($M_W = 6.6$) was also felt by the population with MMI of IV–V in Bima city. In addition, the recent 2018 Lombok sequence resulted in severe damages and claimed >550 casualties (Yang et al., 2020). The 1979 earthquakes also caused severe damages and claimed 37 casualties. Even with $M_W < 7$, earthquakes occurring along the Flores Thrust can have a high seismic hazard. In addition, large earthquakes along the Flores Thrust, such as the 1992 Flores event ($M_W = 7.7$), caused severe damage and generated

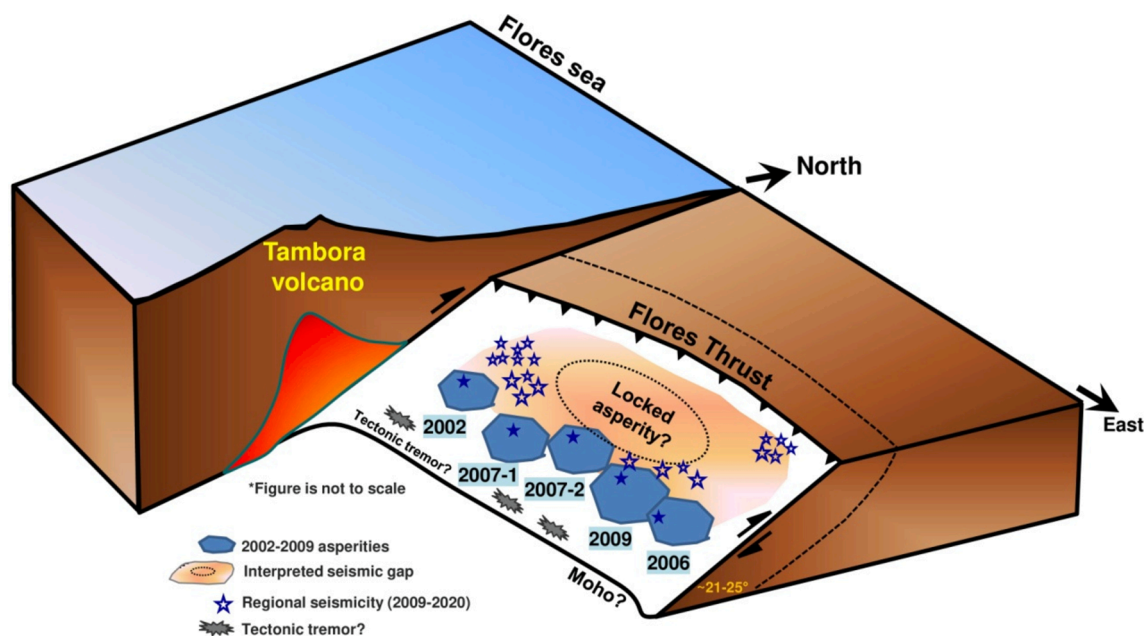


Fig. 17. Tectonic cartoon showing the fault geometry, the interpretation of the five cascading asperities (2002–2009), regional seismicity, and the possible seismic gap in the east of Tambora volcano, Sumbawa.

a large tsunami (Pranantyo and Cummins, 2019).

To consider a candidate event with $M_W > 7$ and to improve future seismic hazard analysis in this region, an earthquake source scaling relation is necessary (Irsyam et al., 2020; Gunawan, 2021; Yulastuti et al., 2021). As shown in Fig. 15, we compared our results with earthquake scaling performed by Yen and Ma (2011) and Cheng et al. (2020) to determine the rupture length– M_W relationship and that performed by Yen and Ma (2011) and Hanks and Bakun (2008) to examine the rupture area– M_W relationship. In general, our results are consistent with source scaling results reported from Taiwan (Yen and Ma, 2011), which mostly consisted of thrust events from the collision zone (Fig. 15).

The results of this study provide the detailed properties of earthquake sources along the Flores Thrust including asperity location, rupture dimension (fault length and width), average slip, rupture speed, and stress drop. This information can contribute to the earthquake source scaling requirement for future regional seismic and tsunami hazards (Irsyam et al., 2020; Yulastuti et al., 2021). Recently, Gunawan (2021) compared published scaling relationships from other locations with seven strike-slip earthquakes and six dip-slip earthquakes from a range of locations and tectonic regimes in Indonesia. No scaling relationship based on finite-fault-rupture models has been established for earthquakes along the Flores Thrust or the eastern Sunda-Banda arc. Based on the successful application of finite-fault rupture models to scaling relationships for specific tectonic regions by Yen and Ma (2011), rupture models obtained in this study can be helpful to determine the source scaling of regional earthquakes along the Flores Thrust. Moreover, the Sumbawa region is a candidate for a nuclear power plant in Indonesia (Yulastuti et al., 2021). Additional studies are necessary to evaluate earthquake and tsunami hazards in this region.

6. Conclusions

We investigated the STFs and possible finite-fault rupture models of five earthquakes ($M_W \geq 6.2$) in the Sumbawa segment of the Flores Thrust. Our source inversions were constrained by teleseismic body and surface waves. Model uncertainties were computed by performing the jackknife test. We observed similar initiation shapes of dynamic rupture for all earthquakes. The ruptures were initiated from the middle crust and often propagated circularly along-strike and down-dip directions. Cascading asperities with a typical low static stress drop ruptured neighboring fault patches, and they did not develop into a single large earthquake with $M_W > 7$. We highlighted that this cascading behavior might be related to the less mature features of the western Flores Thrust. Alternatively, the shallower part of the fault segment could have resulted in a large earthquake, similar to those in the eastern part of the Flores Thrust. Rupture models obtained in this study can be helpful for the source scaling of specific regional earthquakes along the Flores Thrust.

CRedit authorship contribution statement

Dimas Sianipar: Data curation, Methodology, Visualization, Formal analysis, Writing – original draft. **Bor-Shouh Huang:** Methodology, Project administration, Supervision, Validation, Writing – review & editing. **Kuo-Fong Ma:** Methodology, Supervision, Validation. **Ming-Che Hsieh:** Methodology, Software. **Po-Fei Chen:** Methodology, Supervision, Validation. **D. Daryono:** Data curation, Supervision.

Declaration of Competing Interest

The authors declare that they have no known competing financial interests or personal relationships that could have appeared to influence the work reported in this paper.

Acknowledgments

The teleseismic and regional data were retrieved from Incorporated Research Institutions for Seismology (IRIS) Global Seismographic Network (GSN), including the French Global Network of Seismological Broadband Stations (G) and GEOFON Program (GE). The earthquake catalog was retrieved from the International Seismological Center (ISC) and the Indonesian Agency for Meteorology, Climatology, and Geophysics (BMKG). We thank Chen Ji (U. C. Santa Barbara) for the finite-fault inversion code. The effective source dimensions were computed using the code obtained from the website <http://equake-rc.info/cers-software/> (last accessed August 2019). The SCARDEC source-time-functions were downloaded from <http://scardec.projects.sismo.ipgp.fr/>. D. S. thanks Chengli Liu for discussions regarding waveform inversion. We thank Haekal Haridhi and Feisal Dirgantara for discussions regarding the tectonic setting of the studied region. In addition, we thank Cong Nghia Nguyen for discussions regarding the empirical Green's function method. We thank the Editor and reviewers for constructive comments and suggestions to improve the quality of this work. All figures were created using generic mapping tools. D. S. received the Taiwan International Graduate Program (TIGP) Ph.D. fellowship to perform this study. This study was partly funded by the Ministry of Science and Technology, Taiwan (MOST 108-2116-M-001-011, MOST 108-2116-M-001-010-MY3, and MOST 109-2119-M-001-011).

Appendix A. Supplementary material

Supplementary data to this article can be found online at <https://doi.org/10.1016/j.jseae.2022.105167>.

References

- Abercrombie, R.E., 2015. Investigating uncertainties in empirical Green's function analysis of earthquake source parameters. *J. Geophys. Res. Solid Earth* 120 (6), 4263–4277.
- Afif, H., Nugraha, A.D., Muzli, M., Widiyanoro, S., Zulfakriza, Z., Wei, S., Sahara, D.P., Riyanto, A., Greenfield, T., Puspito, N.T., Priyono, A., Samsi, A.T., Supendi, P., Ardianto, A., Syahbana, D.K., Rosalia, S., Cipta, A., Husni, Y.M., 2021. Local earthquake tomography of the source region of the 2018 Lombok earthquake sequence, Indonesia. *Geophys. J. Int.* 226 (3), 1814–1823.
- Allmann, B.P., Shearer, P.M., 2009. Global variations of stress drop for moderate to large earthquakes. *J. Geophys. Res. Solid Earth* 114, B01310.
- Bassin, C., Laske, G., Masters, G., 2000. The current limits of resolution for surface wave tomography in North America. *EOS Trans AGU* 81, F897.
- Beckers, J., Lay, T., 1995. Very broadband seismic analysis of the 1992 Flores, Indonesia, earthquake ($M_w = 7.9$). *J. Geophys. Res. Solid Earth* 100 (B9), 18179–18193.
- Cheng, J., Rong, Y., Magistrale, H., Chen, G., Xu, X., 2020. Earthquake rupture scaling relations for mainland China. *Seismol. Res. Lett.* 91 (1), 248–261.
- Chouet, A., Vallée, M., Causse, M., Courboulès, F., 2018. Global catalog of earthquake rupture velocities shows anticorrelation between stress drop and rupture velocity. *Tectonophysics* 733, 148–158.
- Colombelli, S., Festa, G., Zollo, A., 2020. Early rupture signals predict the final earthquake size. *Geophys. J. Int.* 223 (1), 692–706.
- Dziewonski, A.M., Anderson, D.L., 1981. Preliminary reference Earth model. *Phys. Earth Planet. Inter.* 25 (4), 297–356.
- Ekström, G., Nettles, M., Dziewoński, A.M., 2012. The global CMT project 2004–2010: Centroid-moment tensors for 13,017 earthquakes. *Phys. Earth Planet. Inter.* 200–201, 1–9.
- Ellsworth, W.L., Beroza, G.C., 1995. Seismic evidence for an earthquake nucleation phase. *Science* 268 (5212), 851–855.
- Engdahl, E.R., Di Giacomo, D., Sakarya, B., Gkaraoui, C.G., Harris, J., Storchak, D.A., 2020. ISC-EHB 1964–2016, an Improved Data Set for Studies of Earth Structure and Global Seismicity. *Earth Space Sci.* 7 (1).
- Fuchs, F., Lupi, M., Miller, S.A., 2014. Remotely triggered nonvolcanic tremor in Sumbawa, Indonesia. *Geophys. Res. Lett.* 41 (12), 4185–4193.
- Gilbert, F., Dziewonski, A.M., 1975. An application of normal mode theory to the retrieval of structural parameters and source mechanisms from seismic spectra. *Philosoph. Trans. Roy. Soc. Lond. Series A, Math. Phys. Sci.* 278 (1280), 187–269.
- Griffin, J., Nguyen, N., Cummins, P., Cipta, A., 2019. Historical earthquakes of the eastern Sunda Arc: Source mechanisms and intensity-based testing of Indonesia's national seismic hazard assessment. *Bull. Seismol. Soc. Am.* 109 (1), 43–65.
- Gunawan, E., 2021. An assessment of earthquake scaling relationships for crustal earthquakes in Indonesia. *Seismol. Res. Lett.* 92, 2490–2497.
- Hall, R., 2012. Late Jurassic-Cenozoic reconstructions of the Indonesian region and the Indian Ocean. *Tectonophysics* 570–571, 1–41.

- Hanks, T.C., Bakun, W.H., 2008. M-log A observations for recent large earthquakes. *Bull. Seismol. Soc. Am.* 98 (1), 490–494.
- Hanks, T.C., Kanamori, H., 1979. A moment magnitude scale. *J. Geophys. Res. Solid Earth* 84 (B5), 2348–2350.
- Hao, J., Ji, C., Wang, W., Yao, Z., 2013. Rupture history of the 2013 Mw 6.6 Lushan earthquake constrained with local strong motion and teleseismic body and surface waves. *Geophys. Res. Lett.* 40 (20), 5371–5376.
- Hartzell, S., Liu, P., Mendoza, C., Ji, C., Larson, K.M., 2007. Stability and uncertainty of finite-fault slip inversions: Application to the 2004 Parkfield, California, earthquake. *Bull. Seismol. Soc. Am.* 97 (6), 1911–1934.
- Hayes, G.P., 2011. Rapid source characterization of the 2011 Mw 9.0 off the Pacific coast of Tohoku earthquake. *Earth Planets Space* 63 (7), 529–534.
- Hayes, G.P., 2017. The finite, kinematic rupture properties of great-sized earthquakes since 1990. *Earth Planet. Sci. Lett.* 468, 94–100.
- Helmberger, D.V., 1983. Theory and application of synthetic seismograms. In: Kanamori, H., Boschi, E. (Eds.), *Earthquakes: Observation Theory and Interpretation*. North-Holland Publishing Company, pp. 174–222.
- Huang, B.-S., 2001. Evidence for azimuthal and temporal variations of the rupture propagation of the 1999 Chi-Chi, Taiwan Earthquake from dense seismic array observations. *Geophys. Res. Lett.* 28 (17), 3377–3380.
- Hubbard, J., Barbot, S., Hill, E.M., Tapponnier, P., 2015. Coseismic slip on shallow décollement megathrusts: Implications for seismic and tsunami hazard. *Earth Sci. Rev.* 141, 45–55.
- Irsyam, M., Cummins, P.R., Asurufik, M., Faizal, L., Natawidjaja, D.H., Widiyantoro, S., Meilano, I., Triyoso, W., Rudiyanto, A., Hidayati, S., Ridwan, M., Hanifa, N.R., Syahbana, A.J., 2020. Development of the 2017 national seismic hazard maps of Indonesia. *Earthq. Spectra* 36 (1 suppl), 112–136.
- Ji, C., Helmberger, D.V., Wald, D.J., Ma, K.F., 2003. Slip history and dynamic implications of the 1999 Chi-Chi, Taiwan, earthquake. *J. Geophys. Res. Solid Earth* 108 (B9), 2412.
- Ji, C., Wald, D.J., Helmberger, D.V., 2002. Source description of the 1999 Hector Mine, California, earthquake, part I: Wavelet domain inversion theory and resolution analysis. *Bull. Seismol. Soc. Am.* 92 (4), 1192–1207.
- Kanamori, H., Anderson, D.L., 1975. Theoretical basis of some empirical relations in seismology. *Bull. Seismol. Soc. Am.* 65 (5), 1073–1095.
- Koulali, A., Susilo, S., McClusky, S., Meilano, I., Cummins, P., Tregoning, P., Lister, G., Efendi, J., Syaifi, M.A., 2016. Crustal strain partitioning and the associated earthquake hazard in the eastern Sunda-Banda Arc. *Geophys. Res. Lett.* 43 (5), 1943–1949.
- Langston, C.A., Helmberger, D.V., 1975. A procedure for modelling shallow dislocation sources. *Geophys. J. Int.* 42 (1), 117–130.
- Lay, T., Kanamori, H., Ammon, C.J., Koper, K.D., Hutko, A.R., Ye, L., Yue, H., Rushing, T.M., 2012. Depth-varying rupture properties of subduction zone megathrust faults. *J. Geophys. Res. Solid Earth* 117 (B4), n/a–n/a.
- Lin, X., Chu, R., Zeng, X., 2019. Rupture processes and Coulomb stress changes of the 2017 Mw 6.5 Jiuzhaiguo and 2013 Mw 6.6 Lushan earthquakes. *Earth Planets Space* 71 (1), 1–15.
- Liu, W., Yao, H., 2018. A new strategy of finite-fault inversion using multiscale waveforms and its application to the 2015 Gorkha, Nepal, earthquake. *Bull. Seismol. Soc. Am.* 108 (4), 1947–1961.
- Lythgoe, K., Muzli, M., Bradley, K., Wang, T., Nugraha, A.D., Zulfakriza, Z., Widiyantoro, S., Wei, S., 2021. Thermal squeezing of the seismogenic zone controlled rupture of the volcano-rooted Flores Thrust. *Sci. Adv.* 7 (5), eabe2348.
- Mai, P.M., Beroza, G.C., 2000. Source scaling properties from finite-fault-rupture models. *Bull. Seismol. Soc. Am.* 90 (3), 604–615.
- Manighetti, I., Mercier, A., De Barros, L., 2021. Fault trace corrugation and segmentation as a measure of fault structural maturity. *Geophys. Res. Lett.* 48 e2021GL095372.
- McCaffrey, R., Nábělek, J., 1984. The geometry of back arc thrusting along the eastern Sunda arc, Indonesia: Constraints from earthquake and gravity data. *J. Geophys. Res. Solid Earth* 89 (B7), 6171–6179.
- McCaffrey, R., Nábělek, J., 1987. Earthquakes, gravity, and the origin of the Bali Basin: An example of a nascent continental fold-and-thrust belt. *J. Geophys. Res. Solid Earth* 92 (B1), 441–460.
- Meier, M.A., Ampuero, J.P., Cochran, E., Page, M., 2021. Apparent earthquake rupture predictability. *Geophys. J. Int.* 225 (1), 657–663.
- Melgar, D., Hayes, G.P., 2019. Characterizing large earthquakes before rupture is complete. *Sci. Adv.* 5 (5), eaav2032.
- Musson, R.M.W., 2012. A provisional catalogue of historical earthquakes in Indonesia. Geological Survey Edinburgh British Open Report OR/12/073, p. 21.
- Neely, J.S., Stein, S., Spencer, B.D., 2020. Large uncertainties in earthquake stress-drop estimates and their tectonic consequences. *Seismol. Res. Lett.* 91 (4), 2320–2329.
- Nishikawa, T., Matsuzawa, T., Ohta, K., Uchida, N., Nishimura, T., Ide, S., 2019. The slow earthquake spectrum in the Japan Trench illuminated by the S-net seafloor observatories. *Science* 365 (6455), 808–813.
- Noda, H., Lapusta, N., Kanamori, H., 2013. Comparison of average stress drop measures for ruptures with heterogeneous stress change and implications for earthquake physics. *Geophys. J. Int.* 193 (3), 1691–1712.
- Perrin, C., Manighetti, I., Ampuero, J.-P., Cappa, F., Gaudemer, Y., 2016. Location of largest earthquake slip and fast rupture controlled by along-strike change in fault structural maturity due to fault growth. *J. Geophys. Res. Solid Earth* 121 (5), 3666–3685.
- Pranantyo, I.R., Cummins, P.R., 2019. Multi-data-type source estimation for the 1992 Flores earthquake and tsunami. *Pure Appl. Geophys.* 176 (7), 2969–2983.
- Pranantyo, I.R., Heidarzadeh, M., Cummins, P.R., 2021. Complex tsunami hazards in eastern Indonesia from seismic and non-seismic sources: Deterministic modelling based on historical and modern data. *Geosci. Lett.* 8 (1), 1–16.
- Prieto, G.A., Parker, R.L., Vernon III, F.L., 2009. A Fortran 90 library for multitaper spectrum analysis. *Comput. Geosci.* 35 (8), 1701–1710.
- Salman, R., Lindsey, E.O., Lythgoe, K.H., Bradley, K., Muzli, M., Yun, S.H., Chin, S.T., Tay, C.W.J., Costa, F., Wei, S., Hill, E.M., 2020. Cascading partial rupture of the Flores Thrust during the 2018 Lombok earthquake sequence, Indonesia. *Seismol. Res. Lett.* 91 (4), 2141–2151.
- Sharma, M.L., Wason, H.R., 1994. Occurrence of low stress drop earthquakes in the Garhwal Himalaya region. *Phys. Earth Planet. Inter.* 85 (3–4), 265–272.
- Shao, G., Ji, C., 2012. What the exercise of the SPICE source inversion validation BlindTest 1 did not tell you. *Geophys. J. Int.* 189 (1), 569–590.
- Shao, G., Li, X., Ji, C., Maeda, T., 2011. Focal mechanism and slip history of the 2011 Mw 9.1 off the Pacific coast of Tohoku Earthquake, constrained with teleseismic body and surface waves. *Earth Planets Space* 63 (7), 559–564.
- Silver, E.A., Reed, D., McCaffrey, R., Joyodiwiryo, Y., 1983. Back arc thrusting in the eastern Sunda arc, Indonesia: A consequence of arc-continent collision. *J. Geophys. Res. Solid Earth* 88 (B9), 7429–7448.
- Somerville, P., Irikura, K., Graves, R., Sawada, S., Wald, D., Abrahamson, N., Iwasaki, Y., Kagawa, T., Smith, N., Kowada, A., 1999. Characterizing crustal earthquake slip models for the prediction of strong ground motion. *Seismol. Res. Lett.* 70 (1), 59–80.
- Taymaz, T., Ganas, A., Yolsal-Çevikbilen, S., Vera, F., Eken, T., Erman, C., Keleş, D., Kapetanidis, V., Valkaniotis, S., Karasante, I., Tsironi, V., Gaebler, P., Melgar, D., Öcalan, T., 2021. Source mechanism and rupture process of the 24 January 2020 Mw 6.7 Doğanol-Sivrice earthquake obtained from seismological waveform analysis and space geodetic observations on the East Anatolian Fault Zone (Turkey). *Tectonophysics* 804, 228745. <https://doi.org/10.1016/j.tecto.2021.228745>.
- Thakur, P., Huang, Y., 2021. Influence of fault zone maturity on fully dynamic earthquake cycles. *Geophys. Res. Lett.* 48 e2021GL094679.
- Tichelaar, B.W., Ruff, L.J., 1989. How good are our best models? Jackknifing, bootstrapping, and earthquake depth. *Eos, Trans. Am. Geophys. Union* 70 (20), 593–606.
- Twardzik, C., Ji, C., 2015. The Mw 7.9 2014 intraplate intermediate-depth Rat Islands earthquake and its relation to regional tectonics. *Earth Planet. Sci. Lett.* 431, 26–35.
- Vallée, M., Douet, V., 2016. A new database of source time functions (STFs) extracted from the SCARDEC method. *Phys. Earth Planet. Inter.* 257, 149–157.
- Wang, C., Wang, X., Xiu, W., Zhang, B., Zhang, G., Liu, P., 2020. Characteristics of the seismogenic faults in the 2018 Lombok, Indonesia, earthquake sequence as revealed by inversion of InSAR measurements. *Seismol. Res. Lett.* 91 (2A), 733–744.
- Wells, D.L., Coppersmith, K.J., 1994. New empirical relationships among magnitude, rupture length, rupture width, rupture area, and surface displacement. *Bull. Seismol. Soc. Am.* 84 (4), 974–1002.
- Yamanaka, Y., Kikuchi, M., 2003. Source process of the recurrent Tokachi-oki earthquake on September 26, 2003, inferred from teleseismic body waves. *Earth Planets Space* 55 (12), e21–e24.
- Yang, X., Singh, S.C., Tripathi, A., 2020. Did the Flores backarc thrust rupture offshore during the 2018 Lombok earthquake sequence in Indonesia? *Geophys. J. Int.* 221 (2), 758–768.
- Ye, L., Lay, T., Kanamori, H., Koper, K.D., 2013. Energy release of the 2013 Mw 8.3 Sea of Okhotsk earthquake and deep slab stress heterogeneity. *Science* 341 (6152), 1380–1384.
- Ye, L., Lay, T., Kanamori, H., Rivera, L., 2016. Rupture characteristics of major and great (Mw ≥ 7.0) megathrust earthquakes from 1990 to 2015: 1. Source parameter scaling relationships. *J. Geophys. Res. Solid Earth* 121 (2), 826–844.
- Yen, Y.-T., Ma, K.-F., 2011. Source-scaling relationship for M 4.6–8.9 earthquakes, specifically for earthquakes in the collision zone of Taiwan. *Bull. Seismol. Soc. Am.* 101 (2), 464–481.
- Yuliastuti, Y., Setiadiyura, T., Wicaksono, A.B., Alhakim, E.E., Suntoko, H., Sunarko, S., 2021. High-resolution probabilistic seismic hazard analysis of West Nusa Tenggara, Indonesia. *J. Seismolog.* 25 (3), 937–948.